Sedimentary Geology 411 (2021) 105804

Contents lists available at ScienceDirect

Sedimentary Geology

journal homepage: www.elsevier.com/locate/sedgeo

The sedimentary architecture of hyperpycnites produced by transient turbulent flows in a shallow lacustrine environment

Luxing Dou [a,b], Jim Best [b,c], Zhidong Bao [a], Jiagen Hou [a,*], Li Zhang [d,*], Yuming Liu [a]

[a] College of Geosciences, China University of Petroleum (Beijing), Beijing 102249, China
[b] Department of Geology, University of Illinois at Urbana-Champaign, Urbana, IL 61801, USA
[c] Departments of Geography and GIS, and Mechanical Science and Engineering and Ven Te Chow Hydrosystems Laboratory, University of Illinois at Urbana-Champaign, Urbana, IL 61801, USA
[d] School of Geosciences, Yangtze University, Wuhan 430100, China

ARTICLE INFO

Article history:
Received 1 September 2020
Received in revised form 5 November 2020
Accepted 6 November 2020
Available online 16 November 2020

Editor: Dr. Brian Jones

Keywords:
Hyperpycnites
Transitional flow
Turbulence modulation
Lacustrine
Nenjiang Formation
Songliao Basin

ABSTRACT

Hyperpycnal flows are river-derived extrabasinal turbidity currents transporting both sand and clay to lacustrine, coastal, shelf and deepwater sedimentary environments. Experimental research in the past twenty years has shown that the presence of clay in sediment-laden flows promotes a transitional behavior between fully turbulent flow and a quasi-laminar plug flow regime. However, to date, most work concerning the fluid dynamic interpretation of lacustrine hyperpycnal flows has been founded on concepts based on fully turbulent flows, and relatively little is known about the influence of clay on the rheological and turbulence characteristics of these flows. With the help of 3D seismic volume and wire-line logging data, the present study undertakes a description and interpretation of subsurface mixed sandstone–mudstone bedforms observed in cores from the Upper Cretaceous Heidimiao Sandstone, Nenjiang Formation, Songliao Basin, NE China. Six lithofacies and five lithofacies associations are recognized from the cores and interpreted as formed under both turbulent and transitional flows. Typical bedforms of transitional flows include large current ripples and low-amplitude bedwaves. The delta-fed shallow lacustrine hyperpycnal flow deposits are characterized by proximal sinuous channels (extending for *c.* 20 km) and lobe deposits (extending for >20 km), showing a fan-like geometry associated with distributary channel extension in the down-dip direction. Basal erosion in the proximal channels is produced by the initial turbulent and turbulence-enhanced transitional flows, with channel infill dominated by upper transitional plug flows or quasi-laminar plug flows. The lobe deposits possess a fan-like geometry with large aspect ratio, and were formed from turbulence-enhanced and lower transitional plug flows. The downdip transformation of sediment-laden flows in the lacustrine basin varies from an initial turbulent flow, via quasi laminar plug flows to upper and lower transitional plug flows, to turbulence enhanced transitional flows. These transitional flows are interpreted to have experienced gradual dilution and deceleration and eventually transformed to turbulent flows in their distal regions. A new model for delta-fed shallow lacustrine hyperpycnal flow deposits is presented incorporating decelerated transitional flows and flow transformations. This new model can aid understanding of the depositional processes of lacustrine transitional flows and the facies distribution of hyperpynal flows in both modern and ancient sediments.

1. Introduction & background

Hyperpycnal flows are extrabasinal sustained turbidity currents generated by river flooding (Wright et al., 1986; Mulder et al., 2003; Zavala and Arcuri, 2016), and their deposits – hyperpycnites – have been documented in both modern environments and the sedimentary rock record (Best et al., 2005; Soyinka and Slatt, 2008; Zhang et al., 2015; Xian et al., 2018). However, the identification and distribution of ancient hyperpycnites is currently the subject of much debate (e.g. Shanmugam, 2018; Feng, 2019; Van Loon et al., 2019; Zavala, 2019). Hyperpycnites can develop inversely graded bases and intrasequence erosional contacts linked to waxing of the flood (Kneller and McCaffrey, 2003; Mulder et al., 2003) and pulsing within the flow (Best et al., 2005). Such hyperpycnal flows have been shown to be common in modern sedimentary environments (Zhang, 2013; Zhang and Scholz, 2015; Corella et al., 2016) and play an important role in transporting sediment to basins. Their deposits may thus be more common in the rock record than has been thought previously, especially in lacustrine basins (Soyinka and Slatt, 2008).

Recent studies have documented the sedimentary characteristics of deep lacustrine hyperpycnites using outcrop and subsurface data (Pan et al., 2017; Yang et al., 2017; Xian et al., 2018). Although deep-water hyperpycnites dominate the literature regarding hyperpycnal flow research, hyperpycnites in shallow water settings also play an important role in predicting the distribution of sedimentary facies (Mutti et al.,

* Corresponding authors.
E-mail addresses: jghou63@hotmail.com (J. Hou), zhangx0522@qq.com (L. Zhang).

https://doi.org/10.1016/j.sedgeo.2020.105804
0037-0738/

2003; Mutti et al., 2007; Steel et al., 2018; Dou et al., 2020). These shallow water turbidites represent the natural link between deltaic deposits and deeper water basinal turbidites (Mutti et al., 2003; Normandeau et al., 2013; Wang et al., 2017). Research concerning the characteristics of shelf fan deposits (Okay et al., 2011; Steel et al., 2018; Huang et al., 2019) has shown that shallow lacustrine hyperpycnites may possess both channelized and lobe deposits, but further research and case studies are required to deepen and refine understanding of these sediments.

In studies of hyperpycnites, most interpretations of the flow dynamics are based on considerations of fully turbulent flows, without fully considering the influence of clay content on the rheological and turbulence characteristics of the flow. However, research over the past twenty years has shown that clay-laden flows may show a transitional behavior between fully turbulent and quasi-laminar plug flows (Baas and Best, 2002; Baas et al., 2011, 2016). These transitional flows may generate a range of unique bedforms (Baas et al., 2019; Peakall et al., 2020; Baas et al., 2020) that may be expected within the deposits of delta-fed hyperpycnal flows with mixed sand–clay loads (Zavala and Arcuri, 2016). However, the effects of such flows are not currently well-incorporated into facies models of hyperpycnal flows and we still possess an incomplete knowledge of the role, and properties, of transitional flows in hyperpycnite deposition.

In order to address these gaps in our knowledge of shallow-water hyperpycnal sediments, the present study examines deposits of the 1st sand bed (the Heidimaio Sandstone) in the third member of the Late Cretaceous Nenjiang Formation (K_2n^3) in the Southern Songliao Basin, China. Deep lacustrine hyperpycnal flow deposits have been documented previously in the Late Cretaceous fluvial-lacustrine succession of the Songliao Basin (Pan et al., 2017), and the present study focuses on mixed sand–mud bedforms in these shallow-water hyperpycnal deposits. Although previous studies have focused on description of the subaqueous distributary channels (Zhao et al., 2012; Li et al., 2016), the dominant flow types of the channel system remain poorly documented and understood. However, subsurface data in the form of 3D seismic data, well logs, and core descriptions provide an opportunity to document the architecture and distribution of shallow lacustrine hyperpycnites that can complement previous field outcrop research.

The principal aims of the present study are thus to: (a) describe the sedimentology and distribution of the delta-fed shallow-water hyperpycnites from proximal to distal locations, and (b) analyze their origin and characteristics of the mixed sand–mud bedforms in these deposits. This data contributes towards an improved understanding and sedimentary model for ancient delta-fed hyperpycnites in shallow lacustrine successions, and in which both transitional and turbulent flows are significant.

2. Geological setting

The Songliao Basin is a large Meso-Cenozoic lacustrine basin in Northeastern China with a NE-SW orientation (Fig. 1A). The basin consists of six first-order tectonic units (Feng et al., 2010; Fig. 1B), including the northern plunge, the central depression, the northeastern, southeastern and southwestern uplifts and the western slope, which have a total area of 2.6×10^5 km^2. The present paper focuses principally on the Qian'an area in the southern Songliao Basin (Fig. 1C). The tectonic evolution of the basin consists of a *syn*-rift stage of late Jurassic and early Cretaceous age, an early Cretaceous post-rift stage and a late Cretaceous structural inversion (Wu et al., 2009; Feng et al., 2010; Li and Liu, 2015). The post-rift phase strata (Fig. 2A) consist of the lower Cretaceous Denglouku Formation (K_1d), Quantou Formation (K_1q) and the Upper Cretaceous Qingshankou (K_2qn), Yaojia (K_2y), Nenjiang (K_2n), Sifangtai (K_2s), and Mingshui (K_2m) Formations.

The stratigraphy of the upper Cretaceous Nenjiang Formation has been shown to be dominated by fluvial-lacustrine environments (Feng et al., 2010), and is divided into five members (Fig. 2A). The 1st member of the Nenjiang Formation (K_2n_1) consists principally of dark mudstones, oil shales and shales of deep lacustrine origin belonging to a transgressive systems tract (TST; Zhang et al., 2011). During depositional period K_2n^1 (Fig. 2A), the area of the paleolake increased, reaching a maximum of $>20 \times 10^4$ km^2 (Zhang et al., 2011). The second and third members of

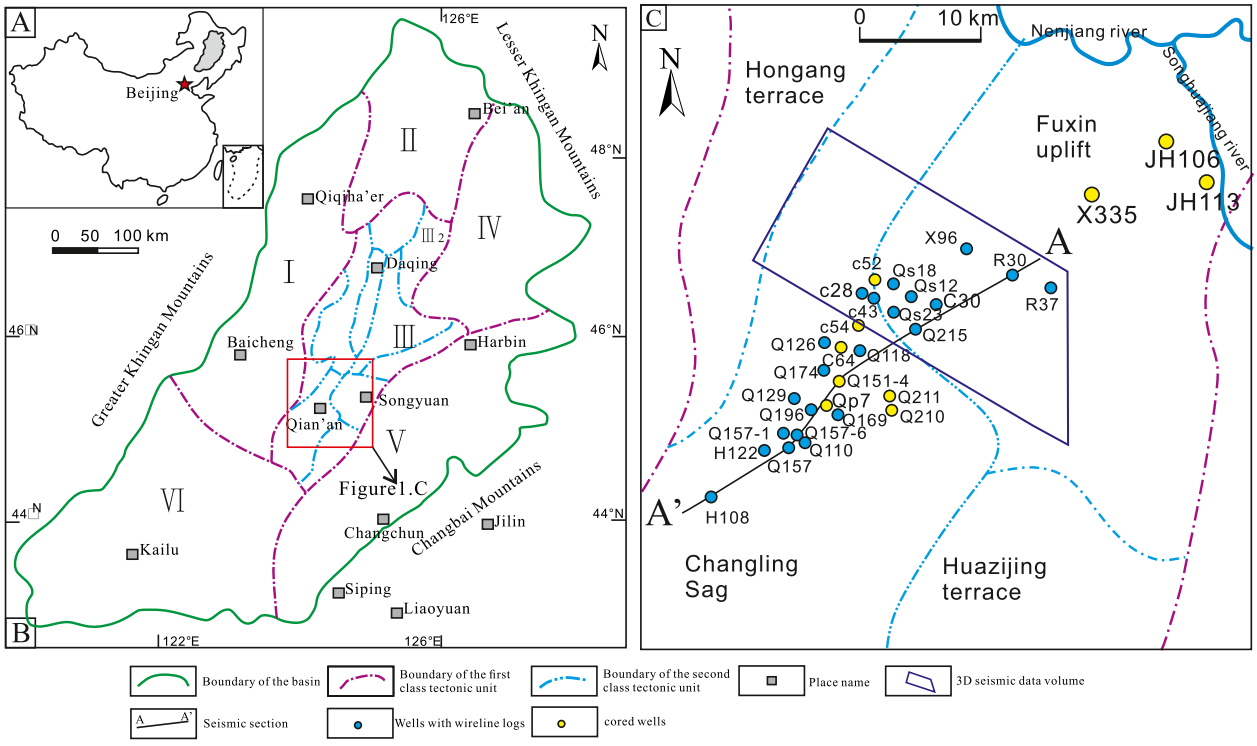

Fig. 1. (A) Location map of the Songliao Basin, NE China. (B) Map showing boundary of tectonic units in the Songliao Basin (modified from Feng et al., 2010). (C) Map showing tectonic units of the southern Songliao Basin, together with well locations and seismic sections detailed in the present study.

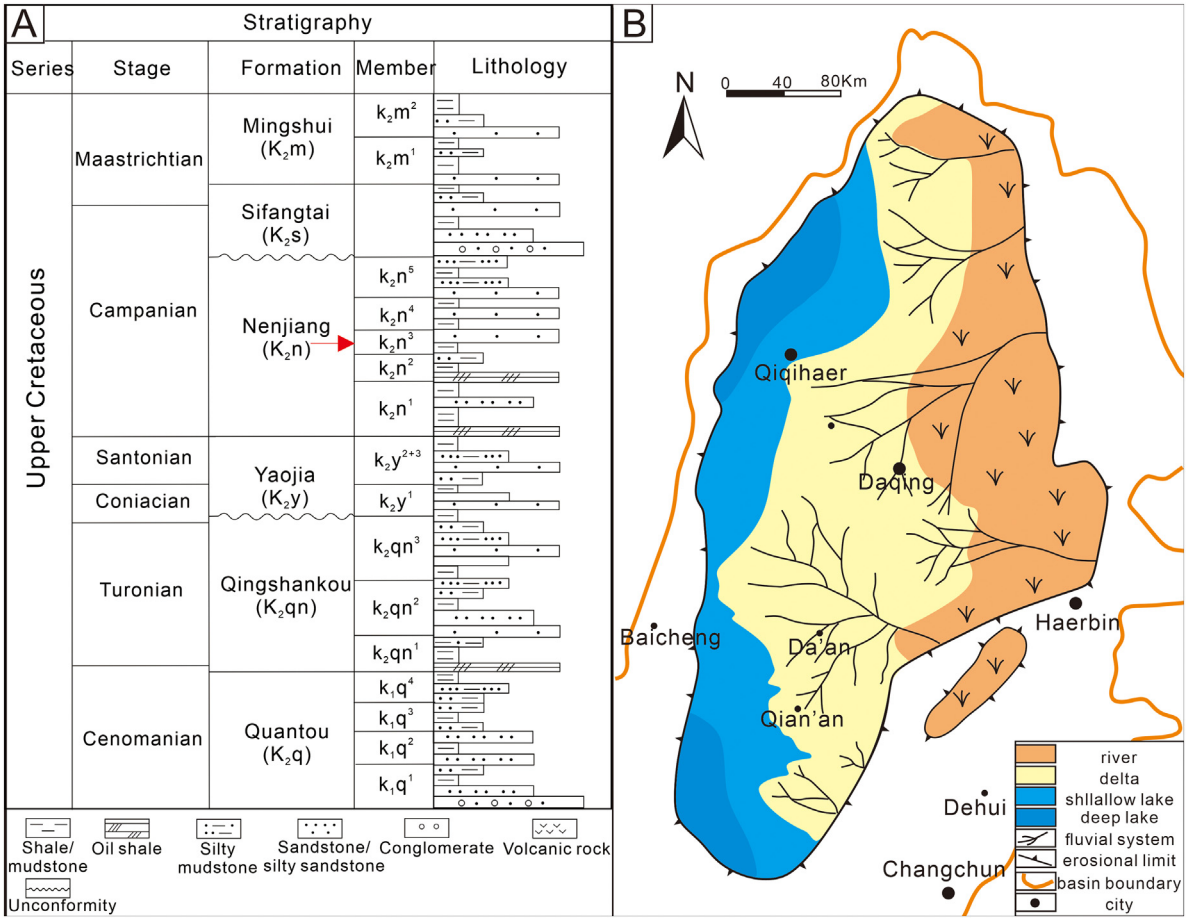

Fig. 2. (A) Simplified stratigraphy of Upper Jurassic - Cretaceous sediments in the Songliao Basin (modified from Wu et al., 2009). (B) Paleogeographic reconstruction of the 3rd member of the Nenjiang Formation (modified from Feng et al., 2010 and Zhang et al., 2015).

the Nenjiang Formation (K_2n^2 and K_2n^3) consist mainly of fluvial-lacustrine sandstones, siltstones and mudstones belonging to a highstand systems tract (Meng et al., 2016) and falling stage systems tract related to a forced regression (Huang et al., 2013; Zhang et al., 2016). In recent years, exploration prospects for hydrocarbon reservoirs in the region were not revealed until the discovery of oil in the Nenjiang Formation Heidimiao Sandstone (K_2n^3, Fig. 2A) in the Qian'an area of the Changling Sag, southern Songliao Basin (Li et al., 2016). These K_2n^3 deposits have been interpreted to have formed in a large fluvial-lacustrine system with a high suspended sediment load derived from the northeast (Fig. 2B; Wang et al., 2014; Mo et al., 2019). A subaqueous channel system has been recognized in the first sandstone bed of the K_2n^3 in the Qian'an area (Wang et al., 2012; Zhao et al., 2012; Li et al., 2016) with a maximum thickness of approximately 15 m. This subaqueous channel system pinches out into thick-bedded lacustrine mudstones and transforms into non-channelized deposits towards the center of the paleolake (Wang et al., 2012). These characteristics thus result in the Nenjiang Formation being suitable for detailing the distribution, and sedimentary architecture, of hyperpycnites derived from a deltaic system in a shallow lacustrine environment.

3. Data and methods

All geological data used in the present study were provided by the Jilin Oil Company, China National Petroleum Corporation. Cores, well logs and 3D seismic data were integrated to document the planform distribution and vertical sedimentary architecture of the shallow lacustrine deposits in the Changling Sag. The methods used in the present study were as follows.

First, 100 m of cores from ten exploration wells (Fig. 1C) of the K_2n^3 interval were described to identify the component lithologies and sedimentary structures (Fig. 3). Lithofacies classification for the ten wells was conducted based on sedimentary structures, texture and grain size, with subsequent interpretation of the depositional flow type based on identification and interpretation of these lithofacies. Second, the distribution of these lithofacies was mapped using seismic sedimentology methods. Well-to-seismic calibration was achieved using a high-precision synthetic seismogram obtained from two 3D seismic surveys (45-Hz dominant-frequency) with a total area of approximately 300 km^2. A 90° phase conversion technique (Zeng and Backus, 2005) and strata slicing technique were used to depict thin-bedded sandbodies on both seismic planform image and profiles. Third, the paleotopography and spatial distribution of lithofacies were mapped by linking the well logs to the seismic profiles. This interpretation of cores and well logs permitted any spatial changes within the different architectural elements to be assessed. Finally, these data and interpretations were used to generate a conceptual model for the different architectural elements, and their changing character from proximal to distal locations, thus aiding in the generic understanding of hyperpycnal flow mechanics and the prediction of sandstone heterogeneity in shallow lacustrine basins.

4. Results

4.1. Lithofacies and interpretation

In the K_2n^3 interval, the succession is composed mainly of well-developed sandstones bounded by dark-colored mudstones (Fig. 3). These muds generally have a hydrogen index (HI) of approximately

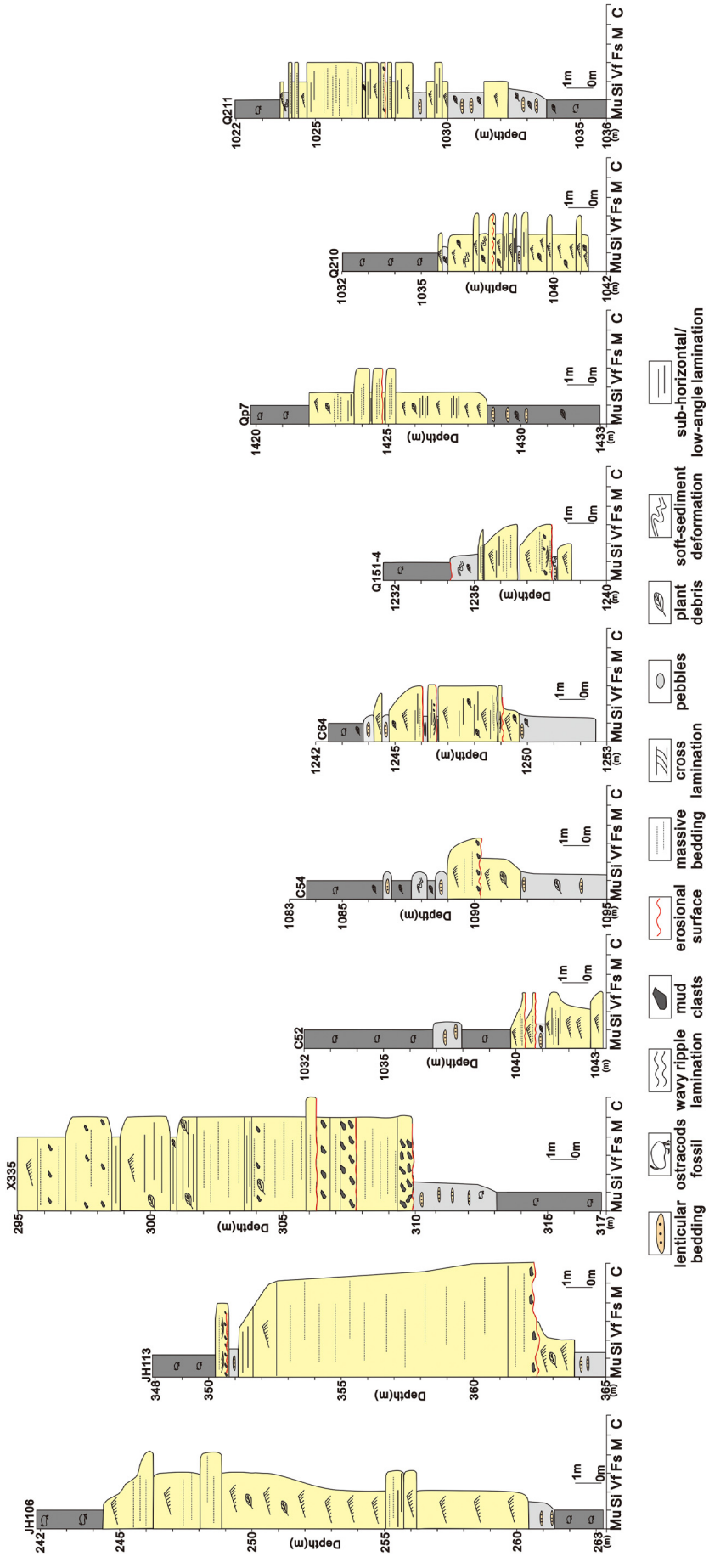

Fig. 3. Sedimentary logs of cores from ten wells, demonstrating the vertical distribution of lithologies and sedimentary structures in the 3rd member of the Nenjiang Formation (K_2n^3).

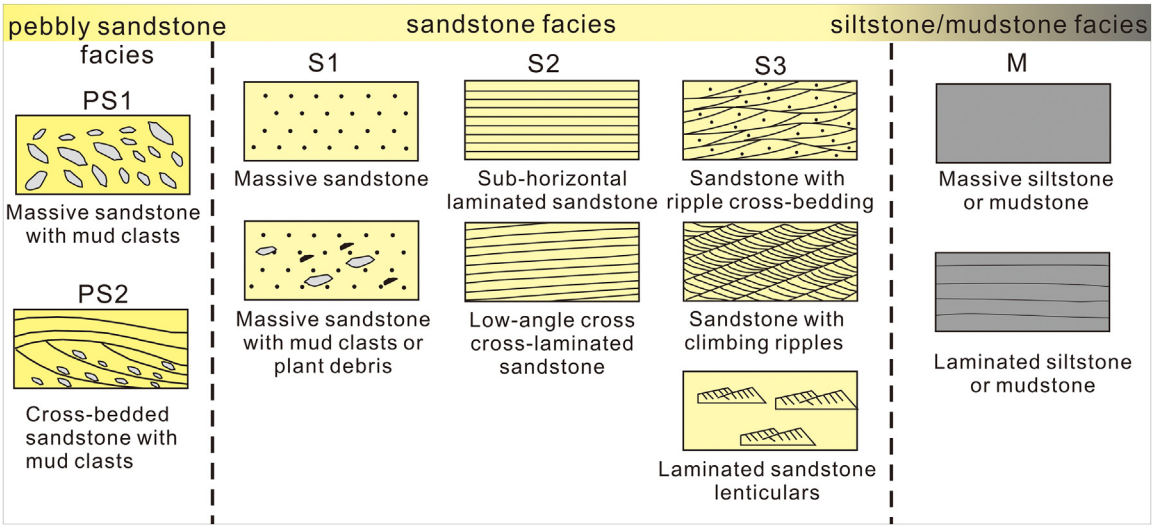

Fig. 4. Lithofacies classification of the 3rd member of the Nenjiang Formation (K_2n^3).

20–300 mg g^{-1}, and have been interpreted to have formed in a shallow lacustrine environment in the Qian'an region (Feng et al., 2010; Zhang et al., 2015). The classification developed herein can be related to the facies classification scheme proposed in previous research by Zavala et al. (2011) and Xian et al. (2018). Six lithofacies were identified from the cores (Fig. 4).

4.1.1. Facies PS1: massive sandstone with mud clasts

4.1.1.1. Description. This lithofacies comprises crudely stratified, dark-colored, mud clasts set in a very-fine to medium grained massive sandstone matrix (Fig. 5A), and is largely present at the base of sandstones. An undulating erosional surface can often be observed at the base of

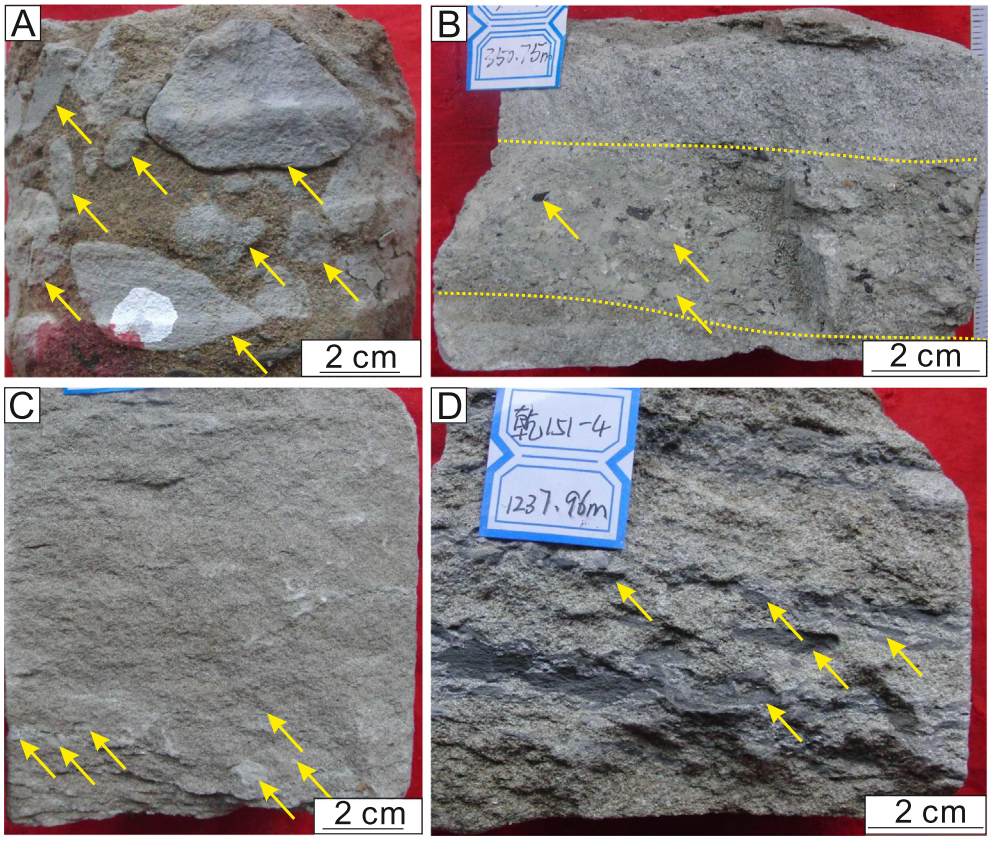

Fig. 5. Representative core photographs of lithofacies PS1 and PS2, with mud clasts highlighted with yellow arrows. All photographs show core viewed from the side, with way-up to the top. (A) Inclined grey mud clasts in lithofacies PS1. Well X335 at 306.28 m. (B) Mud clast layers in sandy deposits in lithofacies PS1. Well JH113 at 350.75 m. (C) Cross-bedded sandstones and inclined grey imbricated mud clasts in lithofacies PS2. Well JH113 at 350.60 m. (D) Cross-bedded sandstones with mud rip-up clasts in lithofacies PS2. Well Q151-4 at 1237.76 m.

this lithofacies (Fig. 5B), with the massive sandstone being moderately to poorly sorted and with a low clay content. The subrounded mud clasts vary greatly in size, from <10 mm to nearly 100 mm or larger, and are often imbricated with a sub-horizontal alignment.

4.1.1.2. Interpretation. This facies is interpreted to be generated by a quasi-laminar plug flow or upper-transitional plug flow (Baas et al., 2016; Baker and Baas, 2020). The rounded, imbricated mud clasts reflect substrate erosion at the bottom of overpassing flows, with these clasts either being sheared within the flow or transported as a basal traction load. This substrate erosion indicates the velocities of the overpassing flows exceeded the erosional threshold of the underlying lacustrine muds (Zavala and Arcuri, 2016), which may have occurred under initially turbulent or transitional flows that could generate erosion, traction and clast abrasion. Such substrate erosion likely increased the clay content in any initially turbulent flows and aided the transformation from turbulent to transitional flows (Baker and Baas, 2020). Clay within the flow may also provide the cohesive forces required to support the sand grains and mud clasts in this facies (Iverson, 1997; Baas et al., 2009, 2011; Talling et al., 2012). In summary, this facies is interpreted as deposits related to concentrated transient turbulent flows.

4.1.2. Facies PS2: cross-bedded sandstone with mud clasts

4.1.2.1. Description. This lithofacies is composed of mud rip-up clasts set in a very fine grained, cross-bedded, sandstone matrix with low-angle (15–20°) inclined laminae (Fig. 5C). The thickness of the cross-lamination is usually greater than 20 mm, and this lithofacies is commonly present at the base of sandstone deposits above an undulating erosional surface. The sandstone is moderately sorted with a low clay content, and with the dark grey mud clasts occurring in the lower part of the cross-bedded sandstone. The mud rip-up clasts range from 2 to

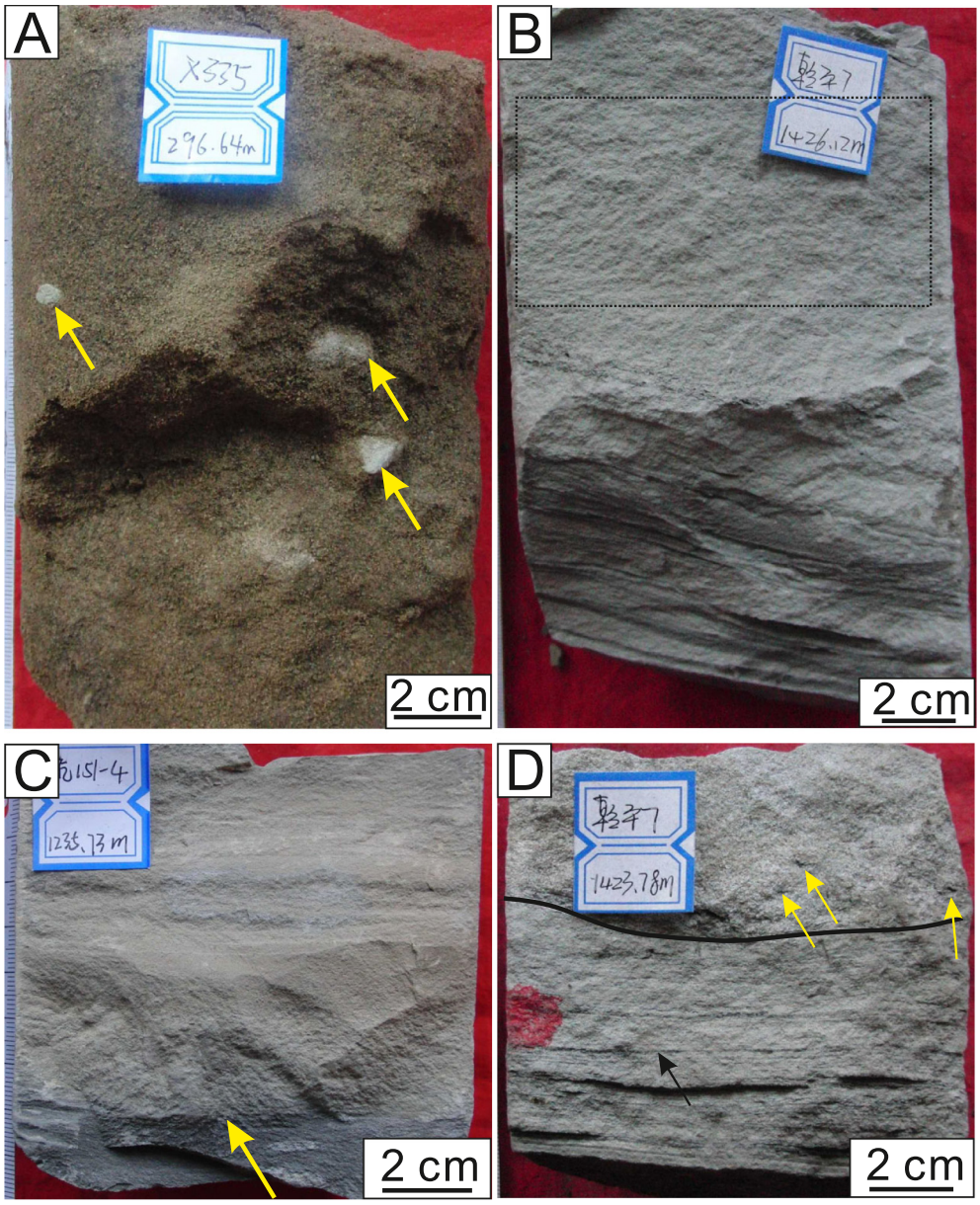

Fig. 6. Representative core photographs of lithofacies S1. (A) Oil-bearing massive sandstone with floating mud clasts (yellow arrows). Well X335 at 296.64 m. (B) Massive sandstone (marked by rectangle) associated with laminated sandstone of facies S2 below. Well Qp7 at 1426.70 m. (C) Sharp-based massive sandstones (yellow arrow) and overlying low-angle lamination showing a fining upward trend. Well Q151-4 at 1235.53 m. (D) Erosive-based massive sandstones with dispersed plant debris (yellow arrows), overlying sandstones with low-angle laminae (Facies S2) separated by a mud layer (black arrow). Well QP7 at 1424.36 m.

20 mm in size (Fig. 5D), and are aligned sub-horizontally in the cross-bedded sandstone matrix. Facies PS2 is usually not developed together with facies PS1.

4.1.2.2. Interpretation. The low-angle cross-stratification indicates bedload transport processes generating bedforms that accumulated small rip-up mud clasts on their lower foresets. These reflect migration of small dunes in a flow that was either fully turbulent, or possibly in a lower transitional plug flow that may act to reduce leeside angles (Baas et al., 2016). However, the lack of clay within the deposits likely points to a flow in which shear was able to overcome the effects of any clays present in the flow. Recent work in fluvial channels (Cisneros et al., 2020; Naqshband and Hoitink, 2020) has revealed the common presence of dune leesides less than the angle-of-repose (and often <15°) and thus in the absence of clay within the sediments, such lower angles may be representative of the natural range in dune leeside angles. The mud rip-up clasts demonstrate erosion and transportation of underlying lacustrine mud deposits, which could increase the clay content in the initially turbulent flows and help the change from turbulent to transitional flows (Baker and Baas, 2020). However, this does not appear significant here and facies PS2, a clay-poor, cross-bedded sandstone with mud clasts, is interpreted as bedload deposits related to turbulent flows.

4.1.3. Facies S1: massive sandstone

4.1.3.1. Description. These massive sandstones comprise greyish or brown, very-fine grained to medium-grained structureless sandstones (Fig. 6A, B), which are characterized by sharp or erosional bases (Fig. 6C, D) and a gradually fining-upward grain size (Fig. 6C). The sandstone is moderately sorted, and low in clay content, with occasional small rounded mud clasts (<20 mm diameter) and carbonaceous plant debris dispersed within the sand matrix (Fig. 6A, D). This lithofacies is usually associated with Facies S2 (Fig. 6B, D).

4.1.3.2. Interpretation. The massive sandstones of Facies S1 are interpreted to indicate rapid deposition of sand under high-

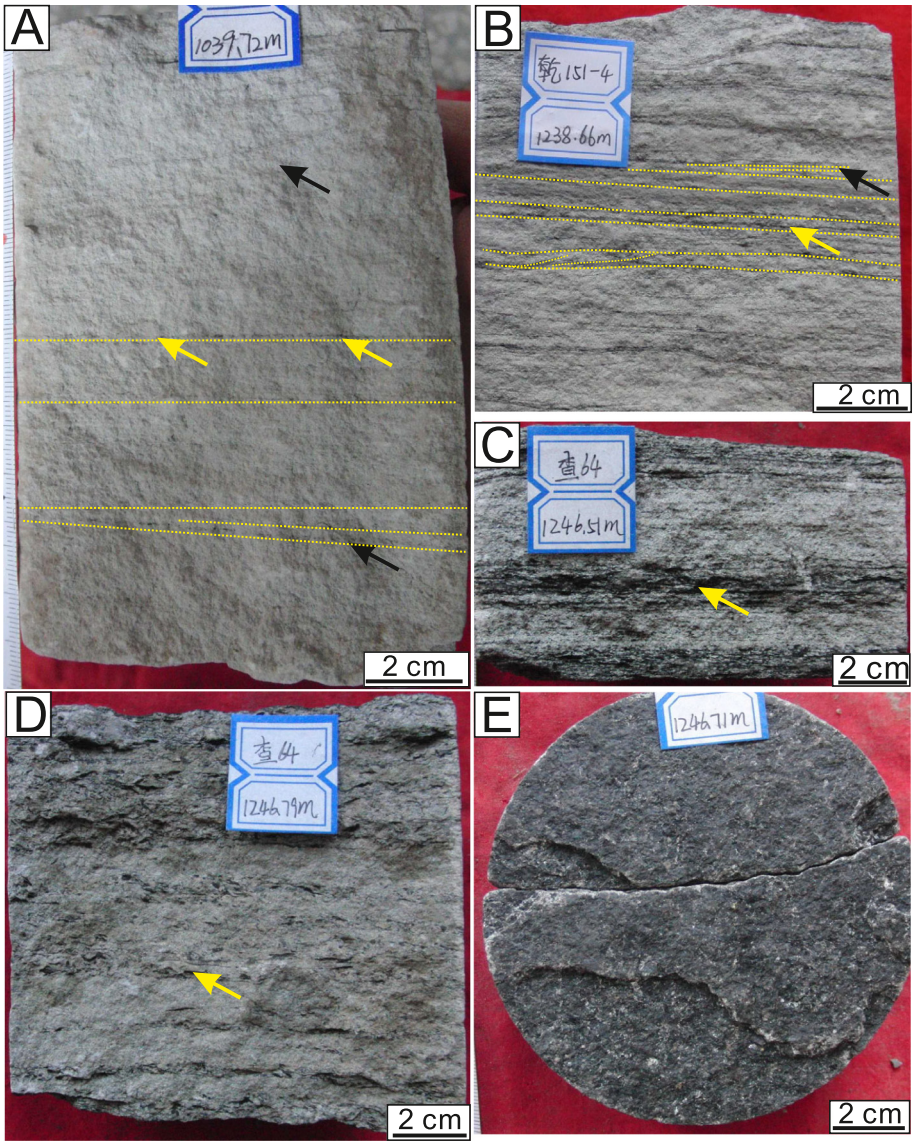

Fig. 7. Representative core photographs of lithofacies S2. (A) sub-horizontal lamination (yellow arrows) and underlying low-angle cross-stratification (black arrow) in sandstones, with the overlying ripple cross-bedding marked by the upper black arrow. Well Q210 at 1039.72 m. (B) Sub-horizontal lamination (yellow arrow) and overlying low-angle cross-stratification (black arrow) in sandstones. Well Q151-4 at 1238.46 m. (C) Plant debris continuously dispersed between laminae in vertical section. Well C64 at 1247.71 m. (D) Plant debris discontinuously dispersed in the sandstones showing sub-horizontal lamination. Well C64 at 1247.99 m. (E) Plant debris between laminae in planform core view. Well C64 at 1247.91 m.

concentration sandy gravity flows that are transitionally turbulent in their behavior (Sanders, 1965; Kneller and Branney, 1995; Baas et al., 2009, 2011; Zavala et al., 2011). The origin of this facies is likely related to progressive aggradation, with fallout rates greater than 0.44 mm s^{-1} as suggested by the experiments of Sumner et al. (2008). This massive sandstone also indicates that these flows possessed insufficient turbulence to generate bedforms, perhaps behaving as an upper transitional plug flow or a quasi-laminar plug flow during flow deceleration (Baas et al., 2009, 2011). The appearance of 'floating' rounded mud clasts within the sandstone indicates the yield strength of the flow was sufficiently high to maintain their transport within these turbulence-damped flows. The sharp bases of these massive sandstones indicate erosion and bypass of sediment by the overlying sediment gravity flows.

4.1.4. Facies S2: laminated sandstone

4.1.4.1. Description. This lithofacies is composed of very-fine grained to medium-grained sandstones with subhorizontal parallel lamination or low-angle (<15°) cross-lamination (Fig. 7A). The laminae are recognized by multiple individual sub-horizontal laminae of millimetric scale, and are usually overlain by climbing ripples (Facies S3; Fig. 7B). The low-angle cross-lamination is recognized by foresets with millimeter-scale low-angle (often 5–15°) laminae (Fig. 7A). Plant debris and mudstones can often be found as a continuous layer between the laminae (Fig. 7B, C), or may be dispersed within the sandstones (Fig. 7D). The abundant plant remains with muds can be seen in planform view of the laminated sandstones in this lithofacies (Fig. 7E).

4.1.4.2. Interpretation. The sub-horizontal and low-angle cross-lamination of Facies S2 have been previously interpreted as the product of traction-plus-fallout processes from fully turbulent flows (Zavala et al., 2006; Xian et al., 2018). However, herein the clay content, sub-horizontal and low-angle cross-lamination are interpreted as the products of decelerating transitional flows (Baas et al., 2016) in which turbulence is attenuated, rather than fully turbulent flows. The low angle of the cross-lamination indicates reduced turbulence and formation of a gently inclined leeside with incorporated clay-rich laminae (Baker and Baas, 2020). Plant debris in such laminated sandstones is commonly considered as evidence of sediment-laden flows related to flood discharge from a terrestrial source (Petter and Steel, 2006; Yoshida et al., 2010; Zavala et al., 2012), which are transported into the basin and trapped on low-angle leeside surfaces. The

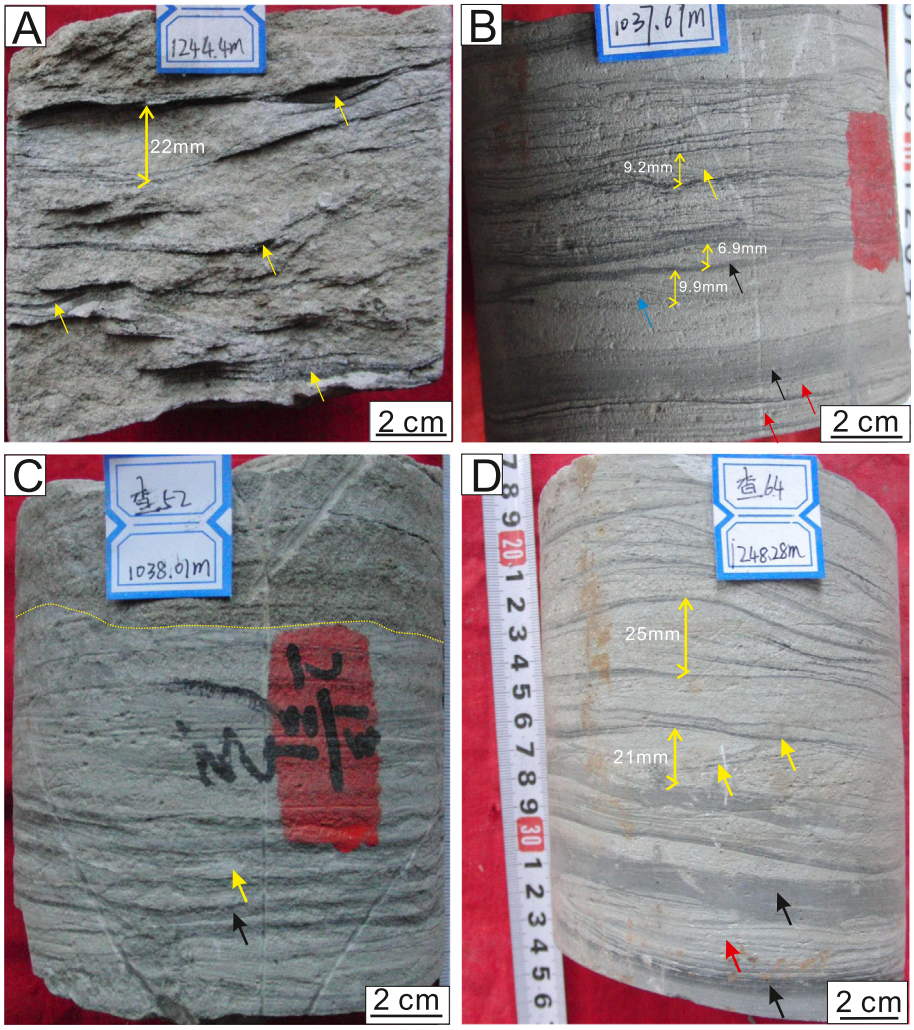

Fig. 8. Representative core photographs of lithofacies S3. (A) Current ripples with asymptotic lower foresets; note the plant debris and mudstone layers with dark colour between the laminae (yellow arrows). The ripple heights are larger than 20 mm. Well C64 at 1245.60 m. (B) Climbing ripples (yellow arrows) and subcritical-climbing current ripples (blue arrow) with mud drapes (black arrow); note the underlying heterolithic beds (red arrows). Ripple heights are <10 mm. Well Q210 at 1037.67 m. (C) Heterolithic strata showing ripple cross-bedding (yellow arrow), and lenticular sands interbedded with mudstone layers (black arrow); note the overlying erosional surface (yellow dotted line). Well C52 at 1040.21 m. (D) Current ripples with mud drapes (yellow arrows), and underlying mudstone layers (black arrows) and heterolithic strata (red arrow) showing low-angle laminae. Well C64 at 1249.48 m.

transition from sub-horizontal, low-angle cross-lamination to overlying ripple cross-bedding suggests a decrease in flow velocity with a consequent increase in the rate of sediment fallout (Sanders, 1965). This transition indicates a decrease in yield strength and/or increase in shear/turbulence within the transitional flows according to the bedform phase diagram of Baas et al. (2016).

4.1.5. Facies S3: sandstone with ripple cross-bedding

This lithofacies comprises very-fine to medium grained greyish sandstones showing ripple cross-bedding with asymptotic lower foresets (Fig. 8A) and climbing ripples (Fig. 8B). They can also develop as heterolithic sandstone with mudstones (Fig. 8C). The heights of individual ripple sets vary from <10 mm (Fig. 8B) to >20 mm (Fig. 8A) and up to 45 mm with a steep lee slope (up to 30°) and gentle stoss slope (Fig. 8B). Abundant plant remains and mudstone layers are also found between the laminae, or filling the trough of these ripple cross-bedded sandstones (Fig. 8A, B, D). This facies thus possesses a mixed sandstone–mudstone texture.

The thin-bedded heterolithic sandstones of Facies S3 are <10 mm in thickness with ripple cross-bedding (Fig. 8C) or low-angle laminae (Fig. 8B, D) showing a characteristic heterolithic nature, with sands interbedded with siltstone and mudstone. This lithofacies is commonly associated with underlying laminated sandstones and interbedded muds (Fig. 8B, D). Facies S3 is also locally associated with underlying mudstone deposits (Fig. 8D) and is commonly eroded by overlying sandstone facies (Fig. 8C).

4.1.5.1. Interpretation. Such current ripples have been previously related to the importance of traction plus fallout processes from waning, fully turbulent flows with a high suspended load (Jopling and Walker, 1968; Mulder and Alexander, 2001; Sumner et al., 2008). Herein, we note that some of these current ripples (Fig. 8A, D) are comparable to the large current ripples of Baas et al. (2011), who noted that ripples greater than 20 mm in height are likely formed under rapidly decelerated turbulence-enhanced transitional flows and lower transitional plug flows. Under such flow conditions with greater yield strengths (*c.* 0.03 to 3 Pa) than clear water flows, near-bed turbulence can be enhanced because the cohesive strength of the flows promotes the development of a near-bed internal shear layer (Baas and Best, 2002; Baas et al., 2009, 2016; Baker and Baas, 2020). This increased turbulence causes the height and wavelength of the current ripples to be greater as compared to sandy current ripples (Baas et al., 2011; Baas et al., 2020). The smaller current ripples of Facies S3, with heights <10 mm, are comparable to the sandy current ripples of Baas et al. (2011) under turbulent flows with less mud content.

The heterolithic cross-bedding displayed by such current ripples has often been interpreted as resulting from alternating phases of waning and waxing flow (Reineck and Wunderlich, 1968; Kneller and Branney, 1995), and such deposits have been documented in turbidites, slurry flow deposits and hybrid event beds (Lowe and Guy, 2000; Haughton et al., 2009; Baas et al., 2011). The mixture of sand and mud within these deposits can also be interpreted as representing deposition from a clay-rich flow, thus developing heterolithic cross-bedding under

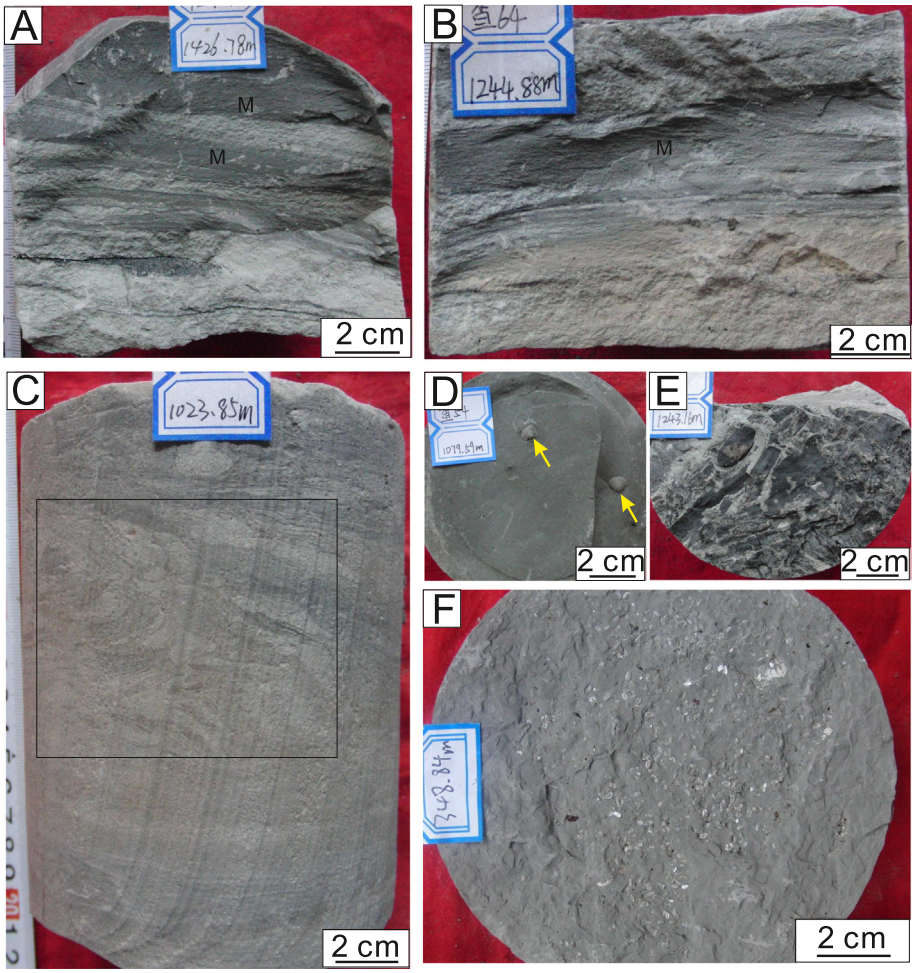

Fig. 9. Representative core photographs of lithofacies M. (A) Mudstone overlying the ripples of facies S3. Well QP7 at 1427.36 m. (B) Laminated silty mudstones overlying ripple cross-bedding. Well C64 at 1246.08 m. (C) Convolute lamination (left side of rectangle) surrounded by mudstone. Well Q211 at 1023.85 m. (D) Bivalve casts in mudstone. Well C54 at 1079.59 m. (E) Plant debris in laminated silty mudstones. Well C64 at 1244.36 m. (F) Abundant ostracods in mudstone. Well JH113 at 348.84 m.

a rapidly decelerated and highly depositional transitional sand-mud gravity flow (Baas et al., 2016). The interbedded plant debris and thicker, horizontal mud layers may also indicate a gradual temporal decrease in flow velocity and settling out of suspension of the fine-grained sediment during temporal velocity pulsing from such sediment-laden flows. Facies S3 often grades horizontally and vertically into the laminated sandstones of facies S2, and was likely controlled by fluctuations in the yield strength of the flows.

4.1.6. Facies M: mudstone

4.1.6.1. Description. This lithofacies comprises massive greyish mudstones, and laminated silty mudstones that usually overlie, or underlie, Facies S3 (Fig. 9A). Heterolithic layers of facies S3 (usually <10 mm in thickness) are often found interbedded with facies M. Soft sediment deformation in the form of convolute lamination (Fig. 9C), the casts of bivalves (Fig. 9D), plant debris (Fig. 9E) and abundant ostracods (Fig. 9F) are found within these massive silty mudstones. The laminated layers of mudstone are usually <10 mm in thickness and bounded by thin (<20 mm) sandstone layers, which may possess terrestrial plant debris.

4.1.6.2. Interpretation. Facies M indicates settling of fine sediment, interpreted here as from the fine-grained tail or suspension cloud of the flows that deposited the sandstones. These fine-grained deposits accumulated as the hyperpycnal flows decelerated and eventually stopped (Patacci et al., 2020). The plant debris dispersed within the mudstones indicates a nearby source of organic material, as well as conditions that allowed settling of this low-density material. These muddy facies indicate quiescent periods between different subaqueous density flows that introduced coarser material into the region (Zavala et al., 2011). The plant debris in this facies likely indicates flood discharges from the fluvial system to the ambient basin water in basin (Lamb et al., 2008; Zavala et al., 2012).

4.1.7. Summary

Based on the observations above, the sandstone beds are interpreted as hyperpycnites produced from hyperpycnal flows triggered by flood events (Mulder and Syvitski, 1995; Zavala and Arcuri, 2016). Four points are worthy of note. First, the deposits provide good evidence for the existence of both turbulent and transitional flows that transported sand, silt and muds in a shallow lacustrine environment from the delta front for tens of kilometers from the Fuxin Uplift to the Changling Sag. Second, the successions display intrasequence erosional contacts that can be explained by waxing of the flood and decelerating transitional sand-mud gravity flow deposits linked to waning of the flood. Temporal pulsing related to hyperpycnal flows (Best et al., 2005) is also revealed from muds interbedded with rippled sandstones. Third, abundant plant debris between the sand laminae provides evidence of transportation by land-derived floods (Petter and Steel, 2006; Zavala et al., 2011). Fourth, the absence of paleosols or mudcracks, and the presence of associated lacustrine microfossils (ostracods), supports the interpretation that the Heidimao sandstone was deposited within a subaqueous environment basinward of the deltaic distributary channels and subaerial delta plain.

4.2. Lithofacies associations

The lithofacies described above can be grouped into five different lithofacies associations (Fig. 10) by analysis of vertical sequences in the cores. Facies association 1 (FA1) comprises facies PS1 at the base, and grades vertically through facies S1, S2, S3 to facies M, showing a fining-upward trend (Fig. 10A). Typical examples of this facies association are present in Wells JH113 and X335 (Fig. 3), which are located at the northeast of the Fuxin Uplift structural belt (Fig. 1B) in the northeast proximal part of the study area, and near the delta front deposits (Wang et al., 2012; Zhao et al., 2012). The abrupt erosional surface and mud clasts near the bottom of FA1 are interpreted to represent the base of channelized deposits in a proximal location of subaqueous sand-mud flows, which were initially turbulent or turbulence-enhanced transitional flows, and triggered by land-derived flood events. Erosion of the fine-grained substrate also likely added mud content to the flows and aided conditions for the transformation from turbulent to transitional flows. The channels are filled by very thick bedded (>5 m) deposits related to decelerating transitional flows.

Facies association 2 (FA2) comprises facies PS2 at the base, and grades vertically from facies S1, S2, S3 to facies M, showing a fining-

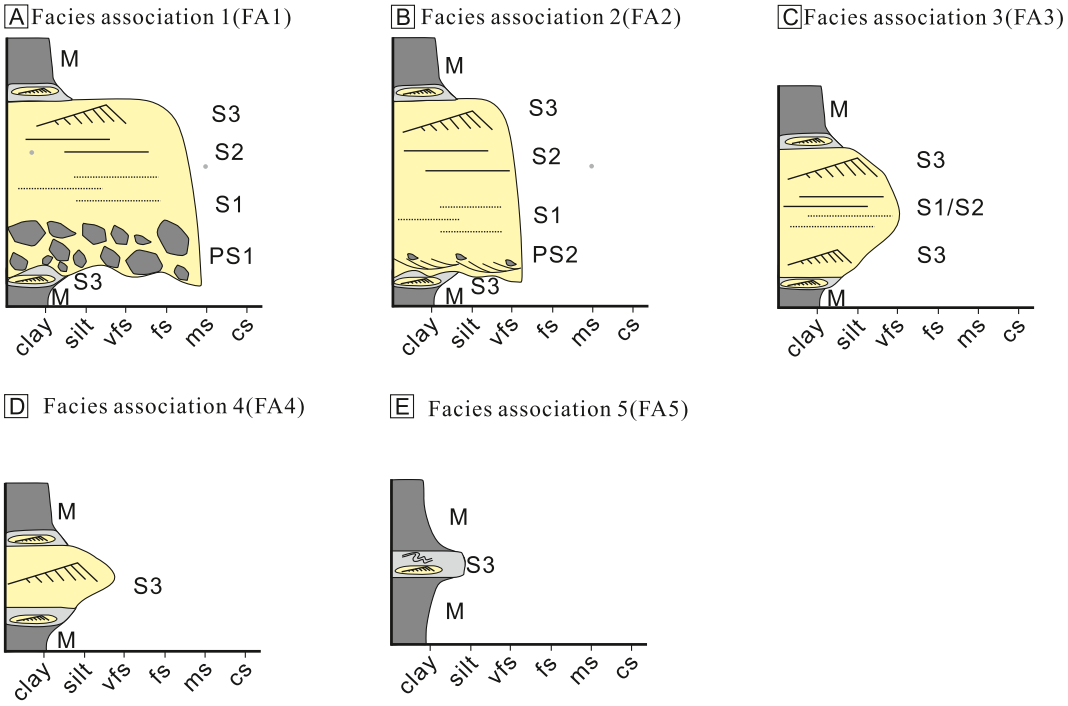

Fig. 10. Classification of facies associations of hyperpycnites in the 3rd member of the Nenjiang Formation (K_2n^3).

upward sequence (Fig. 10B). This facies association is shown in Well Q151-4 that is located at the northeast of the Changling Sag (Fig. 1B), nearly 30 km from proximal Well X335. The mud clasts in facies PS2, and the erosional surface at its base, also provide evidence for erosion and deposition by a turbulent flow. The overlying deposits comprise thick bedded to very thick bedded (~1–3 m) deposits related to decelerating transitional flows. The diameter of the mud clasts is less than within the proximal channel deposits to the northeast, and this could indicate lessening basal shear stresses in decelerating transitional flows in the downflow direction.

Facies association 3 (FA3) comprises facies M at the base, and grades vertically through facies S3, S1 or S2, S3 to facies M, showing first a coarsening-upwards followed by a fining-upwards trend (Fig. 10C). This facies association is shown in Well Q211, Qp7 (Fig. 1B). The flows that produced FA3 were most likely predominantly depositional as inferred from the absence of any strong basal erosion. The coarsening- and then fining- upwards units are interpreted as produced by waxing and waning discharge periods of hyperpycnal flows (Mulder and Alexander, 2001). The transition between these two units corresponds to the maximum grain size and marks approximately the peak of the flood (Mulder et al., 2003). Thus, this facies association indicates thick bedded to very thick bedded (~1–3 m) deposits related to acceleration and deceleration phases of transitional flows that were characterized by large current ripples (Baas et al., 2016; Baker and Baas, 2020; Baas et al., 2020), and turbulent flows producing smaller ripples.

Facies associations 4 (FA4) and 5 (FA5) comprise facies M at the base, and grade vertically from facies S3 to facies M, showing a coarsening-upward followed by a fining-upward cycle (Fig. 10D, E). Facies S3 in FA4 comprises heterolithic bedding and large current ripples in very fine grained sandstones. However, in FA5, facies S3 is mainly composed of interbedded heterolithic bedding in very fine sandstone, surrounded by siltstone and mudstone. Soft sediment deformation, in the form of convolute lamination, is common in FA5. The heterolithic bedding in FA5 is interpreted as indicating alternating deposition of sand from a diluting hyperpycnal current and its muddy suspension cloud. Facies associations FA4 and FA5 are present in Wells Q211, C52 and C54 (Fig. 1B). This thin-thick bedded (~0.2–1 m) facies association, and the absence of facies PS and basal erosion in FA4 and FA5, indicates predominantly depositional transitional flows. Thus FA4 and FA5 are interpreted to indicate suspended- and bed- load dominated deposition from the fine-grained tail or suspension cloud in distal regions of decelerating turbulent flows.

4.3. Distribution and sedimentary architecture of the K_2n^3 sandstones

4.3.1. Geographic distribution

Using the synthetic seismogram derived from sonic wireline log curves, the wells and wireline log curves of the K_2n^3 member can be tied to the 3D seismic data. The seismic data have been flattened on the bottom of the 2nd member of the Nenjiang Formation to reveal changes in depositional gradient and thickness of the 1st sand bed of the K_2n^3 member in seismic profile A-A′ across the Fuxin Uplift and Changing Sag (Fig. 11). This profile shows a gentle slope along the paleoflow direction (NE-SW) with an average gradient <0.5°. In addition, there is a decrease in the gradient of this gentle slope from well R30 in a south-westward direction.

4.3.2. Distributary pattern of sandstones from proximal to distal locations

The planview distribution of sandstones from proximal to distal locations can be examined using a seismic slice and profiles tied to the

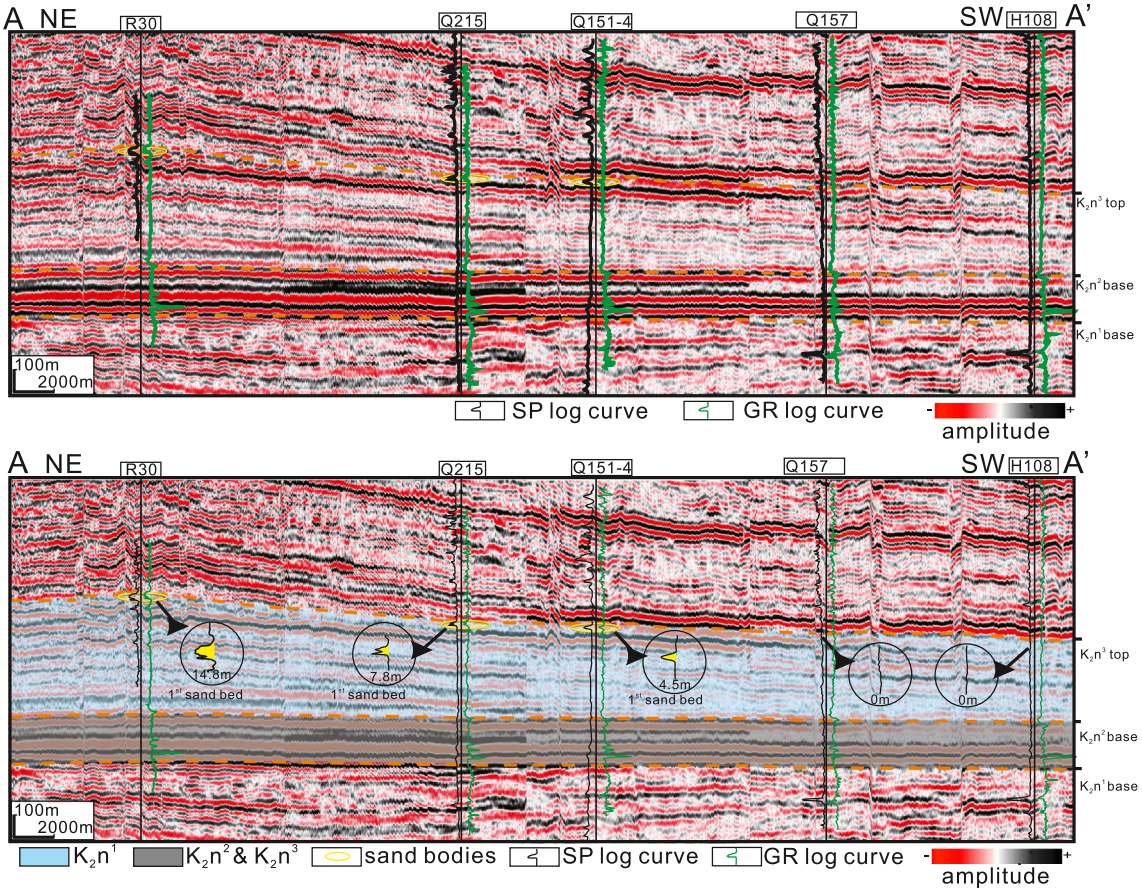

Fig. 11. Vertical seismic panel (A-A′) with well log curves, showing the depositional gradient and thickness variation of the 1st sand bed of the K_2n^3 member in a NE-SW direction (see location of profile in Fig. 1B). The seismic profile has been flattened on the bottom of the K_2n^2 member.

wells. The planform shape of the 1st sand bed of the K_2n^3 member was identified from images of the amplitude attribute slice in the 90° phase-shifted 3D seismic volume (Fig. 12A). The vertical seismic reflection characteristics of these sandbeds were also examined through 90° phase-shifted seismic profiles (Fig. 12B, C).

Channel deposits are clearly defined from the high-amplitude belt in the amplitude attribute slice (Fig. 12A), with these high-amplitude planview reflections showing erosional characteristics in vertical seismic profiles, and a bell shape in the wireline log curves (e.g. Well R30; Fig. 12B). The wireline log curves also show a similar shape in the cored well (X335, Fig. 13). From the log profiles constrained to the wells, the high-amplitude reflection is associated with thick (>9 m) sandstones in the 1st sand bed of the K_2n^3 member (e.g. Well Qs18, 9.6 m). As the reflection weakens in the downflow direction, due to limited seismic resolution of the sandstone, the thickness of the channel sandstones most probably decreases. This can also be seen clearly from sandstone thickness in three wells drilled through the channels along the flow direction: well R30: 14.8 m, well Qs18: 9.6 m, and well C43: 4.9 m (see locations in Fig. 12A).

The distribution of channels shows a complex pattern (Fig. 12A), with two main sinuous channels (width > 1000 m) feeding multiple smaller-scale distributary channels (width < 1000 m) that appear to bifurcate from the main channel. The width of the smaller-scale distributary channels decreases from >800 m to <500 m in the downflow direction (see width measurements in Fig. 12A). The width/depth ratio (W/D) along one distributary channel increases after bifurcation, from 80 in well Qs18 to 131 in well C43.

These seismic data provide evidence of the existence and spatial distribution of channelized deposits in the proximal regions of this depositional system. From the variation of width and thickness, the channels become shallower as channelized incision becomes less in a downflow direction. As the sandstones become thinner downdip, there eventually becomes no obvious reflection of channels recognized in the seismic profiles in the downflow direction. The spatial distribution of the sandstones in these areas was then identified from description and interpretation of the wireline logs, as well as the vertical sequence of sands in the cores using profiles tied to these wells. The distribution of channel sandstones in the downflow direction (Fig. 13) suggests a depositional lobe geometry extending for nearly 50 km. The sandstone lobes then transform into lacustrine mudstone deposits in the distal area (Well H108, Fig. 13). The sandstone thickness in the N-S profile (Fig. 13) shows the lobe possesses thicker sandstones in the proximal area. The thickness of the sand beds decreases in the downflow and lateral directions, and is commonly <6 m. The sandstone thickness in the lobe margin is <4 m (Wells Qp7, Q196, Fig. 13).

In addition, the prominent basal erosion surface found in the proximal channelized sandstones is absent at the bottom of the distal sand beds, although intrasequence erosional contacts are present. This latter characteristic can be found in both cored and non-cored wells from the wireline log curves. In the cored wells, the intrasequence erosional contacts can be clearly defined from variations in lithofacies in the sedimentary logs (Wells C54, C64; Fig. 3). In non-cored wells, the wireline log curves that are related to the sand and mud content can be used to examine the variation in the vertical depositional sequence. Compared to the cylinder-shape gamma log and bell-shape spontaneous potential log curves of channelized deposits in the proximal area (e.g. Wells X335, R30, Qs 18; Fig. 13), the wireline log curves display an egg-shape (e.g. Well C54, Fig. 13) and funnel-shape in these distal areas (e.g. Well Q196; Fig. 13).

Gradual change in the wireline log curves is common within the lobe deposits (e.g. Well C54; Fig. 13) and is different from the abrupt changes in the log curves for the channel deposits of the 1st sand bed (e.g. Well R30; Fig. 13). The egg-shape log curves indicate a compound coarsening- and fining- upward sequence (e.g. Well C54; Fig. 13), which may have intrasequence erosional contacts. The funnel-shape curves indicate a coarsening-upward sequence in the distal fringe of the sand beds as they grade to mudstone deposits (e.g. Well H108; Fig. 13).

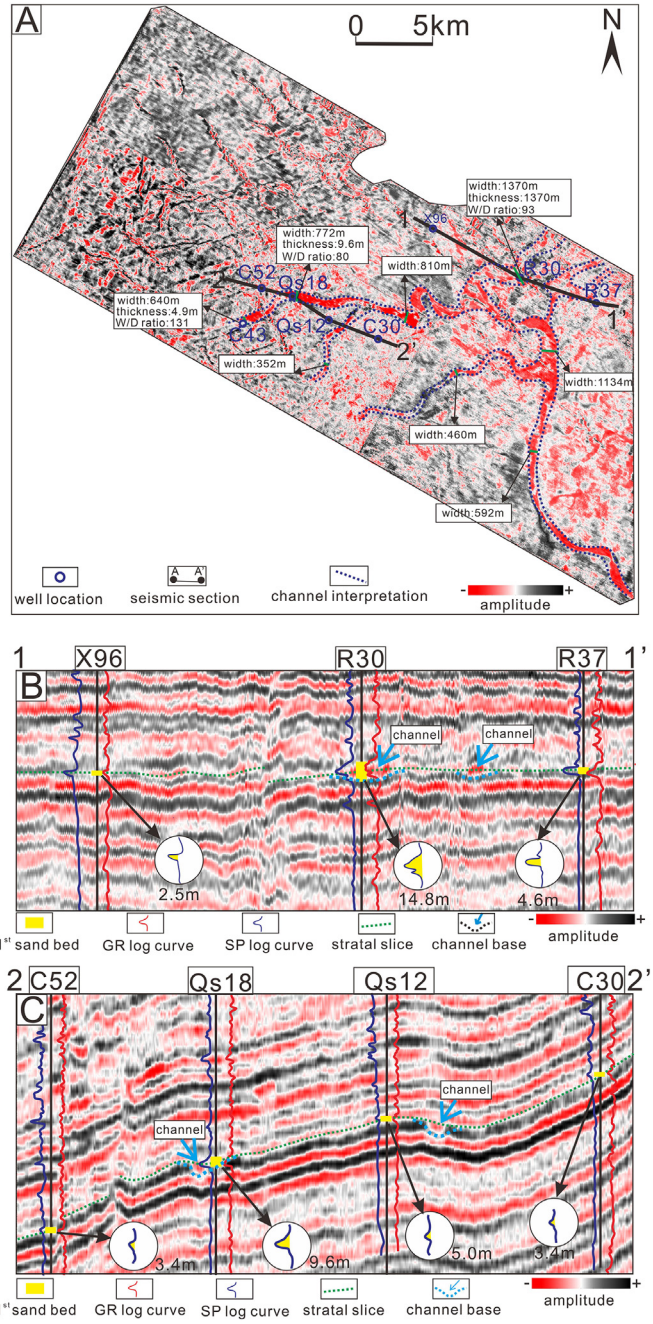

Fig. 12. Distribution of the 1st sand bed of the K_2n^3 member revealed in seismic data. (A) Stratal slice of the 1st sandstone of K_2n^3 through the 3D seismic volume, showing the distributary pattern of the channelized deposits with positive amplitudes. (B) and (C) Vertical seismic profiles (1-1′ and 2-2′ in Fig. 12A) with overlain wireline log curves illustrating the seismic character of channels in the 1st sandstone of K_2n^3.

The absence of basal erosion in the more distal sediments coincides with the channelized deposits transforming into lobe deposits in a down-dip direction. The proximal channels fed sands and muds to the distal lobes and rarely eroded these underlying lobe deposits. The intrasequence erosional contacts are interpreted to indicate the extension of erosive flows from the proximal channels into the lobe deposits during the waxing period of floods.

The lateral variation in sedimentary architecture within the lobe deposits can be further examined in the multiple well-tied profiles for the 1st sand bed in the K_2n^3 member. These show that the proximal

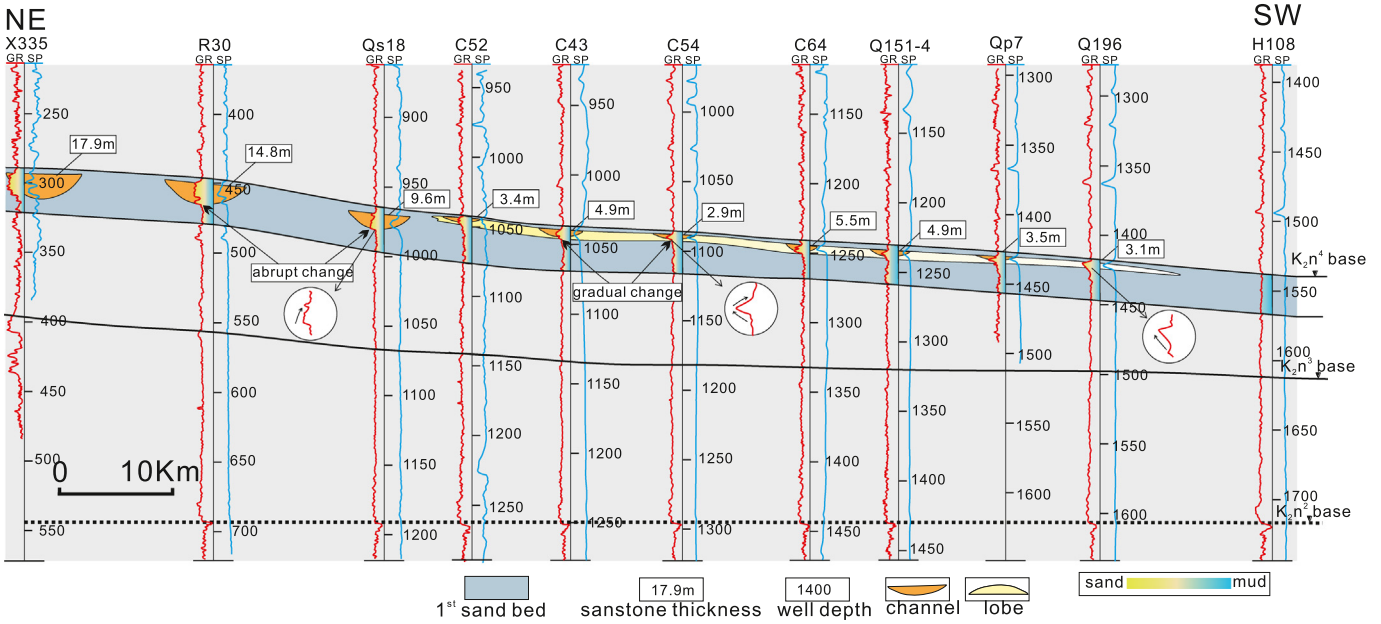

Fig. 13. North-south cross-section with multiple wells, illustrating changes in sandstone thickness towards the southwest. Sand-rich channels occur in the northeast and gradually are replaced by extensive sand-rich lobes near Well Qs18 (see location of section, Fig. 1B).

channelized deposits (Well Qs18; Fig. 14) transform gradually into non-channelized deposits (Well C54; Fig. 14) towards the downflow direction. The extension of the proximal channels into the lobe deposits is also interpreted from the log curves from the cored wells (Well C64, Q151-4; Fig. 14) and non-cored wells (Q169; Fig. 14). The channelized deposits in the lobe become thinner in a downflow direction and disappear in the distal fringe of the lobe deposits (Well Q157-6; Fig. 14). The channels in the lobes also vary laterally into thinner lobe deposits without any channel deposits or intrasequence erosion (Wells Q126, 118; Fig. 14). The sandstone thickness of the lobe is <6 m and its lateral extent is likely >5 km (e.g. C28-Qs23; Fig. 14). This yields an aspect ratio (width to maximum thickness) for the lobes of approximately 1000:1 or larger for this fan-like geometry.

Thus, the distributary channel can be interpreted as having fed sediment to the distal lobes. As the incision depth of the channel deposits varies greatly (e.g. C54 and C64; Fig. 14) and the incision can be found in multiple wells from sections perpendicular to the flow direction (e.g. Q129-Q169; Fig. 14), the channel deposits most likely extend and diverge as an extended terminal 'distributary-like' geometry in the lobe complex and incise into the underlying lobes. The channels terminate at the distal lobe fringe (before well Q196; Fig. 14).

5. Discussion: a depositional model of lacustrine hyperpycnites dominated by transitional turbulent flows

Previous studies have demonstrated that hyperpycnal flow deposits can be well preserved in lacustrine environments (Pan et al., 2017; Yang et al., 2017; Xian et al., 2018), and the present study describes delta-fed hyperpycnal flow deposits in the shallow lacustrine environment of the Late Cretaceous Nenjiang Formation, during which the paleoclimate was mainly semi-arid and semi-humid (Wang et al., 2013; Yang et al., 2020). As such, flood-related hyperpycnal flows are more likely triggered by the high discharge variability under these climates (Petter and Steel, 2006; Zaman et al., 2012; Long, 2017).

Most previous interpretations of hyperpycnal flows have been based on knowledge of bedform dynamics in clearwater turbulent flows (Sanders, 1965; Kuenen, 1966; Kneller and McCaffrey, 2003; Sumner et al., 2008). However, recent research has shown that as the clay content changes, the rheological and turbulence characteristics of sediment-laden flows become modulated (Baas and Best, 2002; Baas et al., 2011, 2016), and thus a fully turbulent flow model may not explain all the flow properties of sand-clay hyperpycnal flows. Such transitional flow properties have been recognized from the interpretation of the hyperpycnites herein, which have been commonly considered deposits formed under solely turbulent flows (Zavala et al., 2011; Xian et al., 2018).

The present research yields a depositional model for hyperpycnal flow deposits in a lacustrine depression (Fig. 15), and here we outline a first attempt to achieve a new perspective in understanding shallow lacustrine hyperpycnal deposits in the light of transitional flows. The model is characterized by proximal channelized deposits and downcurrent lobe deposits associated with distributary channels (Fig. 15A).

In proximal positions, channelized deposits with strong basal erosion develop in a position basinward of the updip delta front deposits (Well X335; Fig. 15B). The main trunk channels are the principal path for sand-clay transport, with minor sinuous distributary channels extending from the main channel. Compared to deltaic distributary channels, these subaqueous channels in the Nenjiang Formation possess relatively few bifurcations (see channel bifurcation near well C30; Fig. 12A).

The seismic data illustrate that the erosional proximal channels likely extend for nearly 20 km from the pro-delta into the shallow lake (Well JH113 to Well Qs18). This channelization was likely produced during the erosion-plus-bypass phase (Zavala et al., 2006) related to periods of increasing flood discharge and continuous acceleration of the hyperpycnal flows. These channels were partially filled with bedload and suspended load sediment transported by waning hyperpycnal flows. The bedload deposits were largely derived from the underlying mud substrate eroded by the overlying initially turbulent and turbulence-enhanced transitional flows. As such, substrate erosion may have increased the clay content of the initial turbulent hyperpycnal flows, generating transitional flows that became the principal sediment-laden flow type in the downdip channels. The channel fill deposits (FA1) were formed during deceleration of transitional flow dominated hyperpycnal events, with sediments in the proximal channels being dominated by massive bedding and low-amplitude bed-waves. These bedforms were likely related to upper transitional plug flows or quasi-laminar plug flows with high yield strength (Baas et al., 2016).

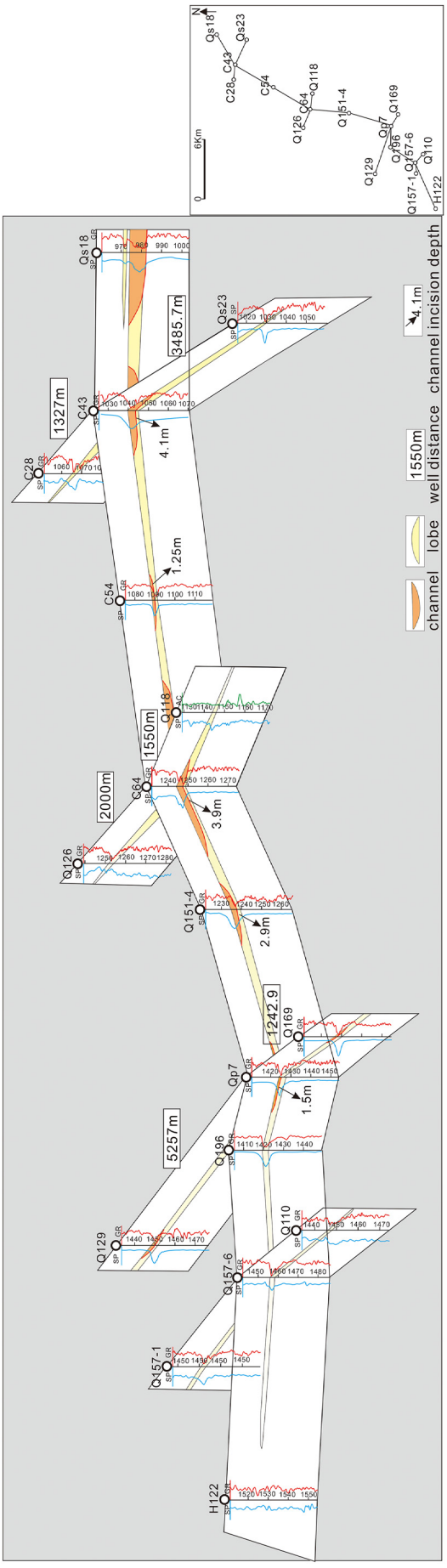

Fig. 14. Three-dimensional fence diagram showing distribution of the 1st sand bed in the K_2n^3 member. The sand beds tend to diverge in the flow direction (to the SW).

The lobe deposits developed in a down-current position from the proximal channelized deposits as the sediment load from the channels expanded in a lobate shape. These lobe deposits extend for >20 km (terminating near Well H122), and possess a fan-like geometry with large aspect ratio (width:depth >1000). The multiple distributary-like channels extended and eroded into the underlying lobe deposits during the erosion-plus-bypass phase. The erosive strength of the flows in the lobe deposits gradually decreases in a downcurrent direction (Fig. 15B). The intrasequence erosion surfaces between the thickening- and thinning- upward sequences in the lobe deposits are interpreted to record waxing-to-waning flood cycles.

During the deceleration phase, both the channel and lobe region between the channels were filled by sandy (FA4) and then muddy (FA5) hyperpycnal flow deposits towards the distal margin of the hyperpycnal dispersal system (Fig. 15B). The dominant bedforms in the lobe deposits are large current ripples and heterolithic stratification comprising alternating laminae or layers of sand and mud, produced under turbulence-enhanced transitional flows and lower transitional plug flows.

Thus, the downdip trend of dominant sedimentary structures varies from massive bedding with mud clasts and low-amplitude bed-waves to large current ripples and heterolithic bedding. This suggests the transitional flows underwent a transformation from proximal channels to downcurrent lobe deposits, from initially turbulent flow derived from the land-derived floods, via quasi-laminar plug flow and upper transitional plug flows to lower transitional plug flow and turbulence-enhanced transitional flows from proximal channels to the downcurrent lobe deposits (Fig. 15C). The flows then decelerated and diluted to transform into turbulent flows in the distal regions (Fig. 15C). This flow transformation was mainly caused by flow deceleration and an increasing clay content during channelization in the proximal area, followed by increasing dilution of the hyperpycnal flows as they mixed with the distal shallow lacustrine ambient water.

The model proposed herein for the internal sedimentary architecture and hyperpycnal flow origin of the shallow lacustrine fan deposits in the Nenjiang Formation (Fig. 14) differs from previous models. The identification and interpretation of bedforms such as large current ripples and low-amplitude bed-waves in the Heidimiao Sandstone suggest that the hyperpycnal flows possessed transitional flow properties in this shallow lake. Hyperpycnal flows have mostly been interpreted as fully turbulent flows in previous research on lacustrine basins (Zavala et al., 2006; Yang et al., 2017; Xian et al., 2018), even although flow velocity and sediment concentration are usually considered the most important factors in bedform evolution formed under such hyperpycnites (Zavala et al., 2006; Zavala et al., 2011). However, as turbulence modulation and bedform generation are also governed by cohesive clay content and the interplay between rheology and shear rate (Baas and Best, 2002; Baas et al., 2011, 2016, 2020), the cohesive clay content must be considered as an additional factor determining bedform evolution and flow transformation within hyperpycnal flows.

The present synthesis suggests that interpretations of hyperpycnites in previous research may require revision to incorporate the importance of transitional flows for hyperpycnite deposition. For example, here we highlight the genetic facies tract (Zavala et al., 2011; Zavala and Pan, 2018) that has been widely applied in previous interpretations of hyperpycnites (Fig. 16A; Steel et al., 2018; Xian et al., 2018; Yang et al., 2020). In the interpretation of this genetic facies tract (Zavala et al., 2011; Xian et al., 2018; Zavala and Pan, 2018), the facies are viewed as depositional products solely of fully turbulent flows, with facies change being dictated by the decline in velocity of the turbulent flow from channels to lobes. This genetic facies tract begins to unravel the complexity of hyperpycnal flow deposits and their depositional processes, but also requires consideration of the flow rheology. In the present study, several facies closely match transitional flow deposits (Fig. 16B) rather than fully turbulent flow deposits. First, some of the massive sandstones in Facies B3s (see figure 9C in Zavala and Pan, 2018) and massive sandstone in Facies S1 (see figure 10 in Zavala and

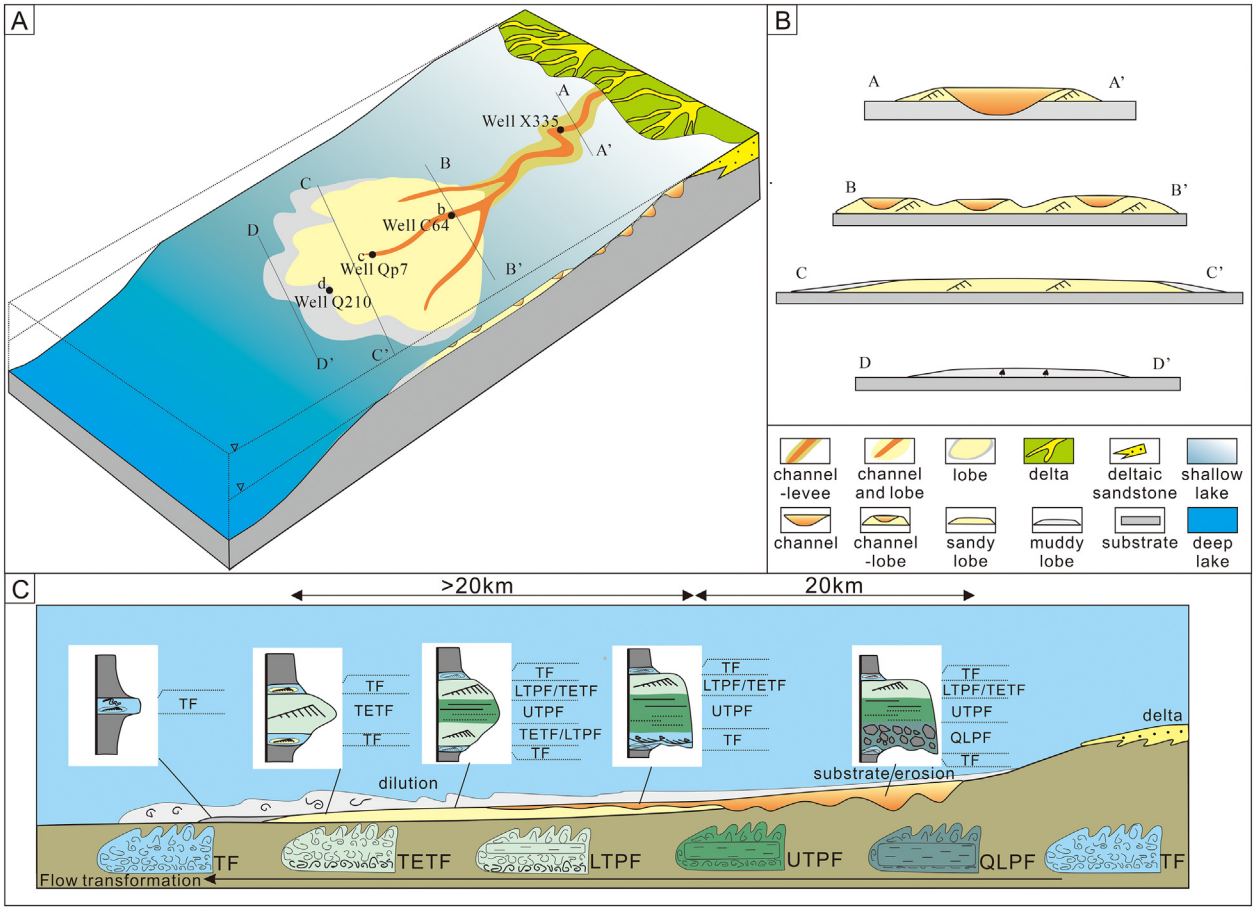

Fig. 15. Conceptual model of transitional flow dominated shallow lacustrine hyperpycnites. (A) Spatial distribution pattern of the hyperpycnite elements. (B) Four sections from proximal to distal showing the sedimentary architecture of the deposits. (C) Schematic model of flow transformation from the proximal to distal fringes of the system, and related vertical transformations. TF, turbulent flow; QLPF, quasi-laminar plug flow; LTPF, lower transitional plug flow; UTPF, upper transitional plug flow; TETF, turbulence-enhanced transitional flow (see Baas et al., 2016 for terminology).

Pan, 2018) share similarities that can be related to an upper transitional plug flow or a quasi-laminar plug flow during flow deceleration (Baas et al., 2009, 2011). Second, Facies S2 (tabular fine-grained sandstone with sub-horizontal parallel lamination or low-angle diverging laminae) in the genetic facies tract (see figure 14 in Zavala and Pan, 2018) is similar to low-amplitude bedwaves formed under upper and lower transitional plug flows (Baas et al., 2011, 2016; Baker and Baas, 2020; Baas et al., 2020). Third, Facies S3 (fine-grained sandstone bodies with climbing ripples) in the genetic facies tract (figure 14A, C in Zavala and Pan, 2018) can also be related to transitional flow deposits. Ripples with individual set thicknesses larger than 20 mm can be found (figure 16C in Zavala and Pan, 2018) with thicknesses up to 50 mm thick (Zavala and Pan, 2018). According to the bedform diagram presented by Baker and Baas (2020; their figure 15), such sand ripples may be large current ripples likely formed under turbulence-enhanced transitional flows (Baas et al., 2011, 2016; Baker and Baas, 2020; Baas et al., 2020). As these facies change from the proximal channel to lobe, they can thus be related to different types of transitional flow (Fig. 16B), with the flows changing in rheology as well as in velocity. In addition, temporal changes in facies represented in vertical sequence also show changing flow type (e.g. facies PS2 formed under turbulent flows from channel deposits in Fig. 16B). Our new model thus recognizes the potential importance of transitional flows in the interpretation of hyperpycnal flow deposits.

For example, in the sedimentary model of Yang et al. (2017), flow transformation from a hyperpycnal flow to debris flow in a deep lacustrine environment was argued to have been triggered by an increase in mud content from erosion of the soft-sediment substrate and natural levees by the hyperpycnal flow. A similar transformation is seen in the present study, but has been interpreted as a transition from an initially turbulent flow to either an upper transitional plug flow or quasi-laminar plug flow. Thus, if hyperpycnites are envisaged as likely possessing a range of transitional flows, there is less need for a dramatic transition in flow rheology from turbulent to debris flow as encapsulated in hybrid event models (Haughton et al., 2009). The debris flow deposits in the model of Yang et al. (2017) may relate to UTPF or QLPF, with flow transformation interpreted more easily as flows with transitional properties that increase in mud content during the erosion of the underlying substrate. In addition, the transitional flow model provides an interpretation of the stacked couplets of thick muds and thin mud-sand mixtures, which may be mistaken for flaser, wavy and lenticular bedding formed under diurnal or semi-diurnal tides (Baas et al., 2016). The new facies framework presented herein may thus aid interpretations of turbulence-modulated, transitional, hyperpycnal flows in both modern and ancient sediments.

6. Conclusions

Using subsurface geological data, delta-fed hyperpycnites in a delta-fed shallow lacustrine environment were recognized in the Late Cretaceous Nenjiang Formation, Songliao Basin, NE China. Based on the description and interpretation of cores, six lithofacies and five lithofacies associations can be recognized and related to a range of hyperpycnal flow types. This interpretation is based principally on: (i) sedimentary structures related to subaqueous turbulent flows and clay-laden transitional flows; (ii) coarsening-upwards sequences

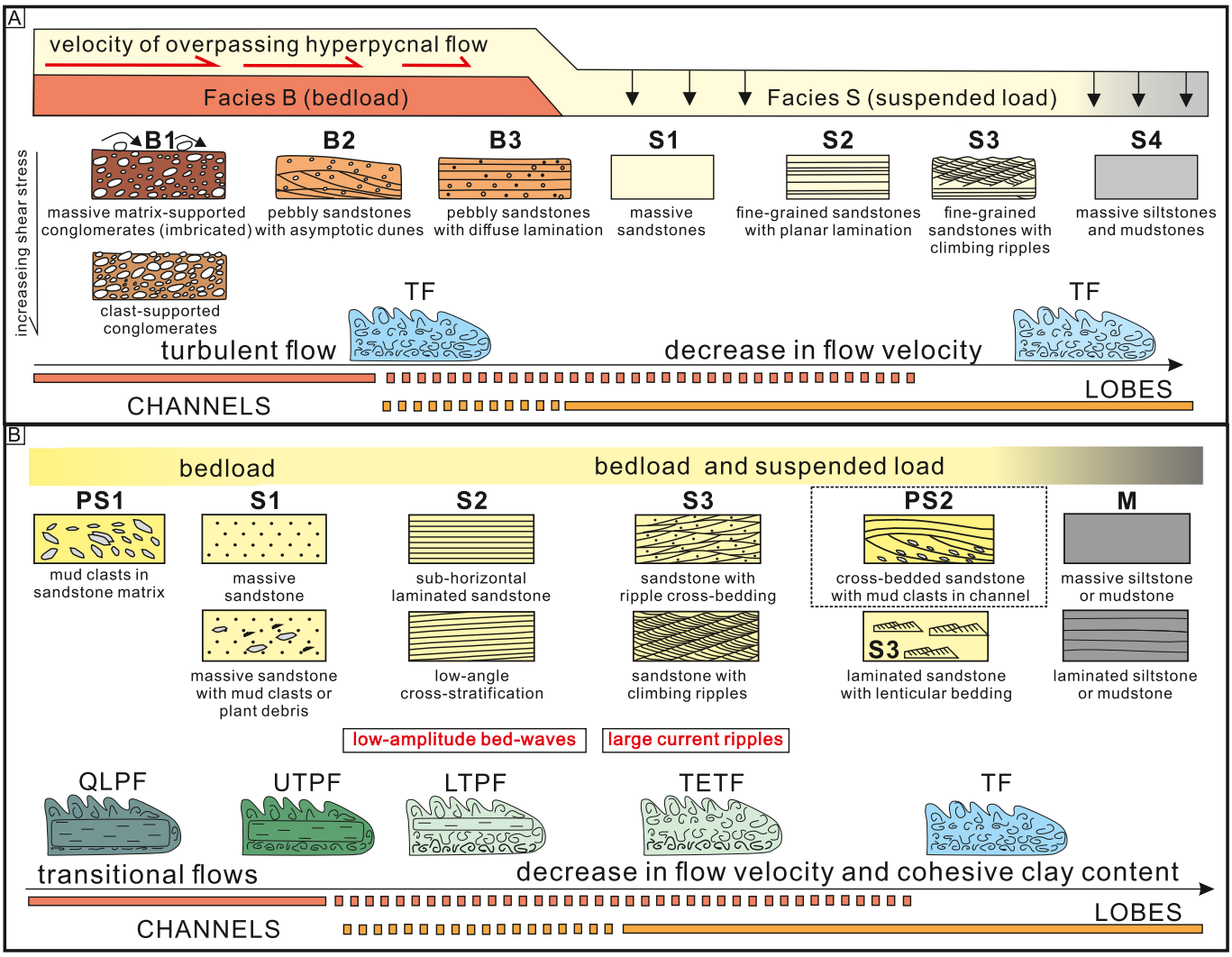

Fig. 16. Schematic genetic facies tract with interpretations based on Zavala et al. (2011) and the present study. (A) Genetic facies tract along a hyperpycnal depositional system controlled by turbulent flows (modified after Zavala et al., 2011; Zavala and Pan, 2018); (B) facies tract along a transitional flow dominated hyperpycnal depositional system in the Nenjiang Formation of the present study. TF, turbulent flow; QLPF, quasi-laminar plug flow; LTPF, lower transitional plug flow; UTPF, upper transitional plug flow; TETF, turbulence-enhanced transitional flow (see Baas et al., 2016 for terminology).

followed by fining-upwards sequences; (iii) abundant plant debris between the sand laminae, and (iv) a subaqueous environment indicated by the absence of paleosols or mudcracks, and the presence of associated lacustrine ostracods.

Characterization of the geometry of these hyperpycnal flow deposits from seismic data reveals a channel to lobe system with complex sedimentary architecture, and that is interpreted to have been generated by sustained hyperpycnal flows from river flood events. The system comprises channelized proximal deposits and downcurrent lobes at its distal margin. The channelized deposits are characterized by locally sinuous major channels and minor channels dominated by high-density hyperpycnal flows eroding into the underlying lacustrine substrate. The hyperpycnal flows show properties of upper transitional plug flows and quasi-laminar plug flows with relatively high clay content and yield strength. The proximal channels transformed downdip to unconfined lobe deposits, which were dominated by lower transitional plug flows and turbulence-enhanced transitional flows in their waning stage. These sediments are characterized by sandy deposits with erosional surfaces interbedded with deposits possessing large current ripples.

The model proposed herein envisages the downdip transformation of dominant sediment-laden flow type in a lacustrine basin progressing from an initial turbulent flow, via quasi-laminar plug flows to upper and lower transitional flows, and then to turbulence-enhanced transitional flows. These transitional flows experienced gradual dilution and eventual deceleration as turbulent flows in a distal lacustrine environment. This model of lacustrine hyperpycnites, dominated by transitional flows, may provide new perspectives for understanding depositional processes in shallow lacustrine sediments, and aiding the prediction of sedimentary heterogeneity in hydrocarbon reservoirs within shallow lacustrine basins.

Declaration of competing interest

The authors declare that they have no known competing financial interests or personal relationships that could have appeared to influence the work reported in this paper.

Acknowledgments

We sincerely thank the Exploration and Development Institute of the Jilin Oilfield, China National Petroleum Corporation, for providing access to the geological and geophysics data. This work was supported by the National Natural Science Foundation of China (Grant No.

41902122), China National Science and Technology Major Project (2016ZX05011-001), the Major State Basic Research Development Program of China (2015CB250901), and the Science Foundation of China University of Petroleum Beijing (No. 2462020YXZZ022). Luxing Dou acknowledges financial support from the China Scholarship Council in a one-year visit to the University of Illinois that permitted writing and completion of this paper.

References

Baas, J.H., Best, J.L., 2002. Turbulence modulation in clay-rich sediment-laden flows and some implications for sediment deposition. Journal of Sedimentary Research 72, 336–340.

Baas, J.H., Best, J.L., Peakall, J., Wang, M., 2009. A phase diagram for turbulent, transitional, and laminar clay suspension flows. Journal of Sedimentary Research 79, 162–183.

Baas, J.H., Best, J.L., Peakall, J., 2011. Depositional processes, bedform development and hybrid flow in rapidly decelerated cohesive (mud-sand) sediment flows. Sedimentology 58, 1953–1987.

Baas, J.H., Best, J.L., Peakall, J., 2016. Predicting bedforms and primary current stratification in cohesive mixtures of mud and sand. Journal of the Geological Society 173, 12–45.

Baas, J.H., Baker, M.L., Malarkey, J., Bass, S.J., Manning, A.J., Hope, J.A., Peakall, J., Lichtman, I.D., Ye, L., Davies, A.G., Parsons, D.R., Paterson, D.M., Thorne, P.D., 2019. Integrating field and laboratory approaches for ripple development in mixed sand–clay–EPS. Sedimentology 66, 2749–2768.

Baas, J.H., Best, J., Peakall, J., 2020. Rapid gravity flow transformation revealed in a single climbing ripple. Geology https://doi.org/10.1130/G48181.1 in press.

Baker, M.L., Baas, J.H., 2020. Mixed sand–mud bedforms produced by transient turbulent flows in the fringe of submarine fans: indicators of flow transformation. Sedimentology https://doi.org/10.1111/sed.12714 (Accept).

Best, J.L., Kostaschuk, R.A., Peakall, J., Villard, P.V., Franklin, M., 2005. Whole flow field dynamics and velocity pulsing within natural sediment-laden underflows. Geology 33 (10), 765–768.

Cisneros, J., Best, J., Dijk, T.V., Almeida, R.P.D., Amsler, M., Boldt, J., Freitas, B., Galeazzi, C., Huizinga, R., Ianniruberto, M., Ma, H., Nittrouer, J.A., Oberg, K., Orfeo, O., Parsons, D., Szupiany, R., Wang, P., Zhang, Y., 2020. Dunes in the world's big rivers are characterized by low-angle lee-side slopes and a complex shape. Nature Geoscience 13, 156–162.

Corella, J.P., Loizeau, J.L., Kremer, K., Hilbe, M., Gerard, J., Dantec, N.L., Girardclos, S., 2016. The role of mass-transport deposits and turbidites in shaping modern lacustrine deep water channels. Marine Petroleum Geology 77, 515–525.

Dou, L.X., Hou, J.G., Song, S.H., Zhang, L., Liu, Y.M., Sun, S., Li, Y.Q., Ren, X.X., Tang, Y., Tian, H., Yang, Y., 2020. Sedimentary characteristics of hyperpycnites in a shallow lacustrine environment: a case study from the Lower Cretaceous Xiguayuan Formation, Luanping Basin, Northeast China. Geological Journal 55 (5), 3344–3360.

Feng, Z.Z., 2019. Words of the Editor-in-Chief: some ideas about the comments and discussions of hyperpycnal flows and hyperpycnites. Journal of Palaeogeography 8 (25), 1–5.

Feng, Z.Q., Jia, C.Z., Xie, X.N., Zhang, S., Feng, Z.H., Timothy, A.C., 2010. Tectonostratigraphic units and stratigraphic sequences of the nonmarine Songliao Basin, northeast China. Basin Research 22, 79–95.

Haughton, P., Davis, C., McCaffrey, W., Barker, S., 2009. Hybrid sediment gravity flow deposits—Classification, origin and significance. Marine and Petroleum Geology 26, 1900–1918.

Huang, W., Zhang, S., Zhang, C., Wei, W., 2013. Sequence configuration and sedimentary evolution of Nenjiang Formation in the Songliao Basin. Acta Sedimentologica Sinica 31 (5), 920–928 (In Chinese with English abstract).

Huang, Y., Yao, G., Fan, X., 2019. Sedimentary characteristics of shallow-marine fans of the Huangliu Formation in the Yinggehai Basin, China. Marine and Petroleum Geology 110, 403–419.

Iverson, R.M., 1997. Physics of debris flows. Reviews of Geophysics 35, 245–296.

Jopling, A.V., Walker, R.G., 1968. Morphology and origin of ripple-drift cross-lamination, with examples from the Pleistocene of Massachusetts. Journal of Sedimentary Research 38, 971–984.

Kneller, B., Branney, M., 1995. Sustained high-density turbidity currents and the deposition of thick massive sands. Sedimentology 42, 607–616.

Kneller, B.C., McCaffrey, W.D., 2003. The interpretation of vertical sequences in turbidite beds: the influence of longitudinal flow structure. Journal of Sedimentary Research 73, 706–713.

Kuenen, P.H., 1966. Experimental turbidite lamination in a circular flume. The Journal of Geology 74 (5), 523–545.

Lamb, M.P., Myrow, P.M., Lukens, C., Houck, K., Strauss, J., 2008. Deposits from wave-influenced turbidity currents: Pennsylvanian Minturn Formation, Colorado, U.S.A. Journal of Sedimentary Research 78, 480–498.

Li, C., Liu, S.F., 2015. Cretaceous anomalous subsidence and its response to dynamic topography in the Songliao Basin, Northeast China. Journal of Asian Earth Sciences 109, 86–99.

Li, X.T., Chen, Q.L., Wu, C.D., Liu, H.Q., Fang, Y.N., 2016. Application of multi-seismic attributes analysis in the study of distributary channels. Marine and Petroleum Geology 75, 192–202.

Long, D.G.F., 2017. Evidence of flash floods in Precambrian gravel dominated ephemeral river deposits. Sedimentary Geology 347, 53–66.

Lowe, D.R., Guy, M., 2000. Slurry-flow deposits in the Britannia Formation (Lower Cretaceous), North Sea: a new perspective on the turbidity current and debris flow problem. Sedimentology 47, 31–70.

Meng, Q., Zhang, S., Sun, G., Fu, X., Chao, W., Yao, S., 2016. A seismic geomorphology study of the fluvial and lacustrine-delta facies of the Cretaceous Quantou-Nenjiang Formations in Songliao Basin, China. Marine and Petroleum Geology 78, 836–847.

Mo, W.L., Wu, C.D., Su, N., Zhang, S., Wang, M.Z., 2019. Seismic imaging of the sedimentary system of the Upper Cretaceous Nenjiang Formation in the Northern Songliao Basin. Journal of Earth Science 30 (4), 788–798.

Mulder, T., Alexander, J., 2001. Abrupt change in slope causes variation in the deposit thickness of concentrated particle-driven density currents. Marine Geology 175 (1), 221–235.

Mulder, T., Syvitski, J.P.M., 1995. Turbidity current generated at river mouths during exceptional discharges to the world oceans. Journal of Geology 103, 285–299.

Mulder, T., Syvitski, J.P.M., Migeon, S., Faugères, J.C., Savoye, B., 2003. Marine hyperpycnal flows: Initiation, behavior and related deposits, a review. Marine Petroleum Geology 20 (6), 861–882.

Mutti, E., Tinterri, R., Benevelli, G., di Biase, D., Cavanna, G., 2003. Deltaic, mixed and turbidite sedimentation of ancient foreland basins. Marine and Petroleum Geology 20, 733–755.

Mutti, E., Tinterri, R., Magalhaes, P.M., Basta, G., 2007. Deep-water turbidites and their equally important shallow-water cousins. Search and Discovery Article AAPG. #50057.

Naqshband, S., Hoitink, A.J.F., 2020. Scale-dependent evanescence of river dunes during discharge extremes. Geophysical Research Letters 47, e2019GL085902.

Normandeau, A., Lajeuness, P., St-Onge, G., 2013. Shallow-water longshore drift-fed submarine fan deposition (Moisie River Delta, Eastern Canada). Geo-Marine Letters 33, 391–403.

Okay, S., Jupinet, B., Lericolais, G., Cifci, G., Morigi, C., 2011. Morphological and stratigraphic investigation of a Holocene subaqueous shelf fan, north of the Istanbul Strait in the Black Sea. Turkish Journal of Earth Sciences 20, 287–305.

Pan, S., Liu, H., Zavala, C., Liu, C., Liang, S., Zhang, Q., Bai, Z., 2017. Sublacustrine hyperpycnal channel-fan system in a large depression basin: a case study of Nen 1 member, Cretaceous Nenjiang formation in the Songliao Basin, NE China. Petroleum Exploration and Development 44 (6), 911–922.

Patacci, M., Marini, M., Felletti, F., Di Giulio, A., Setti, M., McCaffrey, W.D., 2020. Origin of mud in turbidites and hybrid event beds: insight from ponded mudstone caps of the astagnola turbidite system (NW Italy). Sedimentology https://doi.org/10.1111/sed.12713.

Peakall, J., Best, J.L., Baas, J.H., Hodgson, D.M., Clare, M.A., Talling, P.J., Dorrell, R.M., Lee, D. R., 2020. An integrated process-based model of flutes and tool marks in deep-water environments: implications for palaeohydraulics, the Bouma sequence and hybrid event beds. Sedimentology https://doi.org/10.1111/sed.12727.

Petter, A.L., Steel, R.J., 2006. Hyperpycnal flow variability and slope organization on an Eocene shelf margin, central basin, Spitsbergen. AAPG Bulletin 90 (10), 1451–1472.

Reineck, H.E., Wunderlich, F., 1968. Classification and origin of flaser and lenticular bedding. Sedimentology 11, 99–104.

Sanders, J.E., 1965. Primary sedimentary structures formed by turbidity currents and related sedimentation mechanisms, Middleton G V. Primary sedimentary structures and their hydrodynamic interpretation. SEPM Special Publication 12, 192–219.

Shanmugam, G., 2018. The hyperpycnite problem. Journal of Palaeogeography 7 (6), 1–42.

Soyinka, O.A., Slatt, R.M., 2008. Identification and micro-stratigraphy of hyperpycnites and turbidites in Cretaceous Lewis Shale, Wyoming. Sedimentology 55 (5), 1117–1133.

Steel, E., Simms, A.R., Steel, R., Olariu, C., 2018. Hyperpycnal delivery of sand to the continental shelf: insights from the Jurassic Lajas Formation, Neuquen Basin, Argentina. Sedimentology 65, 2149–2170.

Sumner, E.J., Amy, L.A., Talling, P.J., 2008. Deposit structure and processes of sand deposition from decelerating sediment suspensions. Journal of Sedimentary Research 78, 529–547.

Talling, P.J., Masson, D.G., Sumner, E.J., Malgesini, G., 2012. Subaqueous sediment density flows: depositional processes and deposit types. Sedimentology 59, 1937–2003.

Van Loon, A.J., Hüneke, H., Mulder, T., 2019. The hyperpycnite problem: comment. Journal of Palaeogeography 8 (24), 1–7. https://doi.org/10.1186/s42501-019-0034-6.

Wang, J.H., Chen, H.H., Jiang, T., Tang, Z.X., Zhao, B.F., Xu, D.H., 2012. Sand bodies frameworks of subaqueous distributary channel in shallow-water delta, Xinli area of Songliao Basin. Earth Science (Journal of China University of Geosciences) 03, 556–564 (In Chinese with English abstract).

Wang, C.S., Feng, Z.Q., Zhang, L.M., Huang, Y.J., Cao, K., Wang, P.J., Zhao, B., 2013. Cretaceous paleogeography and paleoclimate and the setting of SKI borehole sites in Songliao Basin, northeast China. Palaeogeography, Palaeoclimatology, Palaeoecology 385, 17–30. https://doi.org/10.1016/j.palaeo.2012.01.030.

Wang, L.X., Wu, C.D., Mo, W.L., Zhang, S., 2014. Sedimentary characteristics and identification of muddy deltaic in Nenjiang Formation of Songliao Basin. Acta Scientiarum Naturalium Universitatis Pekinensis 50 (3), 497–506 (in Chinese with English abstract).

Wang, J.H., Xie, X., Pang, X., Liu, B., 2017. Storm-reworked shallow-marine fans in the Middle Triassic Baise area, South China. Sedimentary Geology 349, 33–45.

Wright, L.D., Yang, Z.S., Bornhold, B.D., Keller, G.H., Prior, D.B., Wiseman Jr, W.J., 1986. Hyperpycnal plumes and plume fronts over the Huanghe (Yellow River) delta front. Geo-Marine Letters 6 (2), 97–105.

Wu, H., Zhang, S., Jiang, G., Huang, Q., 2009. The floating astronomical time scale for the terrestrial Late Cretaceous Qingshankou Formation from the Songliao Basin of Northeast China and its stratigraphic and paleoclimate implications. Earth Planetary Science Letters 278 (3), 308–323.

Xian, B., Wang, J., Gong, C., Yin, Y., Chao, C., Liu, J., Yan, Q., 2018. Classification and sedimentary characteristics of lacustrine hyperpycnal channels: triassic outcrops in the south Ordos Basin, central China. Sedimentary Geology 368, 68–82.
Yang, R.C., Jin, Z.J., Van Loon, A.J., Han, Z.Z., Fan, A.P., 2017. Climatic and tectonic controls of lacustrine hyperpycnite origination in the Late Triassic Ordos Basin, central China: implications for unconventional petroleum development. AAPG Bulletin 101 (1), 95–117.
Yang, H.F., Huang, Y.J., Ma, C., Zhang, Z.F., Wang, C.S., 2020. Recognition of Milankovitch cycles in XRF core-scanning records of the Late Cretaceous Nenjiang Formation from the Songliao Basin (northeastern China) and their paleoclimate implications. Journal of Asian Earth Sciences 194, 104183. https://doi.org/10.1016/j.jseaes.2019.104183.
Yoshida, M., Yoshiuchi, Y., Hoyanagi, K., 2010. Occurrence conditions of hyperpycnal flows, and their significance for organic-matter sedimentation in a Holocene estuary, Niigata Plain, Central Japan. Island Arc 18 (2), 320–332.
Zaman, M.A., Rahman, A., Haddad, K., 2012. Regional flood frequency analysis in arid regions: a case study for Australia. Journal of Hydrology 475 (4), 74–83.
Zavala, C., 2019. The new knowledge is written on sedimentary rocks: a comment on Shanmugam's paper "the hyperpycnite problem". Journal of Palaeogeography 8 (23), 1–8.
Zavala, C., Arcuri, M., 2016. Intrabasinal and extrabasinal turbidites: origin and distinctive characteristics. Sedimentary Geology 337, 36–54.
Zavala, C., Pan, S.X., 2018. Hyperpycnal flows and hyperpycnites: origin and distinctive characteristics. Lithologic Reservoirs 30 (1), 1–27.
Zavala, C., Ponce, J., Drittanti, D., Arcuri, M., Freije, H., Asensio, M., 2006. Ancient lacustrine hyperpycnites: a depositional model from a case study in the Rayoso Formation (Cretaceous) of west-central Argentina. Journal of Sedimentary Research 76, 41–59.
Zavala, C., Arcuri, M., Gamero, H., Contreras, C., Di Meglio, M., 2011. A genetic facies tract for the analysis of sustained hyperpycnal flow deposits. In: Slatt, R.M., Zavala, C. (Eds.), Sediment Transfer From Shelf to Deep Water—Revisiting the Delivery System. 61. AAPG Studies in Geology. American Association of Petroleum Geologists (AAPG), Tulsa, Oklahoma, U.S.A, pp. 31–51.
Zavala, C., Arcuri, M., Valiente, L.B., 2012. The importance of plant remains as diagnostic criteria for the recognition of ancient hyperpycnites. Revue de Paléobiologie, Genève 11 (6), 457 446.
Zeng, H., Backus, M.M., 2005. Interpretive advantages of 90° phase wavelets: part 1-modeling. Geophysics 70 (3), C7–C15.
Zhang, X., 2013. Climatic control of the Late Quaternary hyperpycnite sedimentology of Lake Kivu, East Africa. Geology 42 (9), 811–814.
Zhang, X., Scholz, C.A., 2015. Turbidite systems of lacustrine rift basins: examples from the Lake Kivu and Lake Albert Rifts, East Africa. Sedimentary Geology 325, 177–191.
Zhang, S., Fu, X.L., Zhang, C.C., 2011. Stratigraphic sequences and sedimentary evolution in the Yaojia and Nenjiang Formations, Songliao basin. Sedimentary. Geology. Tethyan Geology 31 (2), 34–42 (In Chinese with English abstract).
Zhang, C.C., Zhang, S., Wei, W., Wu, C.D., 2015. The mechanism and significance of the cretaceous condensed section in the Nenjiang Formation, Songliao basin. Acta Sedimentologica Sinica 33 (5), 891–898 (In Chinese with English abstract).
Zhang, C.C., Wei, W., Zhang, S., Wu, C.D., Fu, X.L., Cui, K.N., 2016. Architecture of lacustrine mass-transport complexes in the Mesozoic Songliao Basin, China. Marine and Petroleum Geology 78, 826–835.
Zhao, B.F., Wang, J.H., Xu, D.H., Xu, M., Jin, X.M., 2012. Semi-quantitative research on subaqueous distributary channel sandbodies of the 3th member of Nenjiang Formation in Xinli-Xinbei Area, Songliao Basin. Acta Sedimentologica Sinica 30 (3), 511–521 (In Chinese with English abstract).